

MATERIALS
CHEMISTRY
FRONTIERS



Interactions between Fullerene Derivatives and Biological Systems

Journal:	<i>Materials Chemistry Frontiers</i>
Manuscript ID	QM-REV-01-2023-000004.R1
Article Type:	Review Article
Date Submitted by the Author:	22-Feb-2023
Complete List of Authors:	Siringan, Mark John; Rutgers University School of Arts and Sciences Dawar, Abhiram; Rutgers University School of Arts and Sciences Zhang, Jianyuan; Rutgers University School of Arts and Sciences,

SCHOLARONE™
Manuscripts

REVIEW

Interactions between Fullerene Derivatives and Biological Systems

Mark John Siringan, Abhiram Dawar and Jianyuan Zhang*

Received 00th January 20xx,
Accepted 00th January 20xx

DOI: 10.1039/x0xx00000x

Attention towards nanoparticles from pharmaceutical and biomedical fields significantly increased due to their attractive surface modification, high drug-loading, and improved pharmacokinetics. Fullerenes, an allotrope of carbon, stand out for their molecularly exact structure, potent radical-scavenging, photoactivatable reactive-oxygen species generation, and ability to definitively confine metal atoms and clusters. Accordingly, fullerene systems have been applied in various biological contexts, including increased and controlled drug delivery, antioxidative, anti-inflammatory, and photodynamic therapy, and magnetic resonance imaging. Ultimately, the pleiotropic activity of fullerenes, coupled with its precise structure and functionalization, can realize precise and tailorable medicines. Different from some excellent reviews focusing on the structure and chemistry of fullerene derivatives and their biomedical applications, this review highlights the interaction of fullerene materials with biological systems, with insight into their structural influence on their interactions with the cellular environment.

1. Introduction

Recent advancements in bottom-up synthesis and fabrication of nanoparticles have yielded powerful biomedical tools to overcome the hurdles within conventional passive/diffusion-based diagnostic and therapeutic approaches with tailorable and multivalent ligands.¹ Within this pool of nanoparticles, fullerenes stand out as a unique elementary building block because their molecular nature can provide the much-needed precision and uniformity in biomedical research that is difficult to achieve in conventional nanoparticles. They also have the added advantage of carbon makeup which matches the carbon-based theme of life, bestowing it greater biocompatibility and lower toxicity compared to many other inorganic nanoparticles. In contrast to its physical and electronic properties, the biological activity of fullerene materials was initially limited in its investigation due to poor aqueous compatibility² and weak absorption of visible light.³ The report of water-soluble fullerene systems opened various avenues of its biological study, and many works have taken advantage of its properties for uses in MR imaging,^{4,5} drug delivery,^{6,7} antiviral and antibacterial defense,^{8,9} antioxidative and anti-inflammatory therapy,^{10–12} photodynamic therapy (PDT),^{13–15} and tumor targeting^{16,17} (Fig. 1). These applications are based upon several fullerene structural features, including its hydrophobicity, large π electron cloud, and ability to act as a robust exohedral and endohedral host.

Considering the prevalence of van der Waals contacts in protein interactions¹⁸ as well as the lipophilic environment of membrane structures, the hydrophobicity of the fullerene cage suggests its utility in membrane and protein targeting. While this hydrophobicity was a significant contributor to the initial roadblock in biological studies, various functionalization strategies have been utilized to bestow water solubility.^{19,20} Non-specific multiaddition to the cage, such as decoration with hydroxyl, carboxyl, or amino groups, allows access to highly-water soluble systems at the expense of loss of conjugation, hydrophobicity, and molecular precision but provides “nanoparticle-like” multivalency. In another category, specific ligand addition, such as through the Diels-Alder, Prato or Bingel-Hirsch reactions,²¹ allows for aqueous compatibility with minimal alteration of the cage. Ultimately, the combination of both water solubility and hydrophobicity led to the design of amphiphilic fullerene systems, which have been investigated in various biological contexts.^{22–24} These fullerene derivatives have been dubbed different names in previous research; for clarity, we summarize the key compounds discussed in this review in Table 1.

The large π -electron cloud is another attractive feature of fullerene nanoparticles. This conjugation results in two appealing properties. The first is that greater conjugation results in low-lying LUMOs,²⁵ which are responsible for the efficient energy acceptance of fullerenes in donor-acceptor dyads.²⁶ The second appeal comes from the ability of the double bonds to react with reactive oxygen species (ROS), thus scavenging them.²⁴ This antioxidant property of fullerenes suppresses oxidative stress that arises from ROS build-up²⁷ and has been shown to attenuate the symptoms of several pathologies.^{12,28,29}

Department of Chemistry and Chemical Biology, Rutgers University, Piscataway, NJ, USA. E-mail: jy.zhang@rutgers.edu

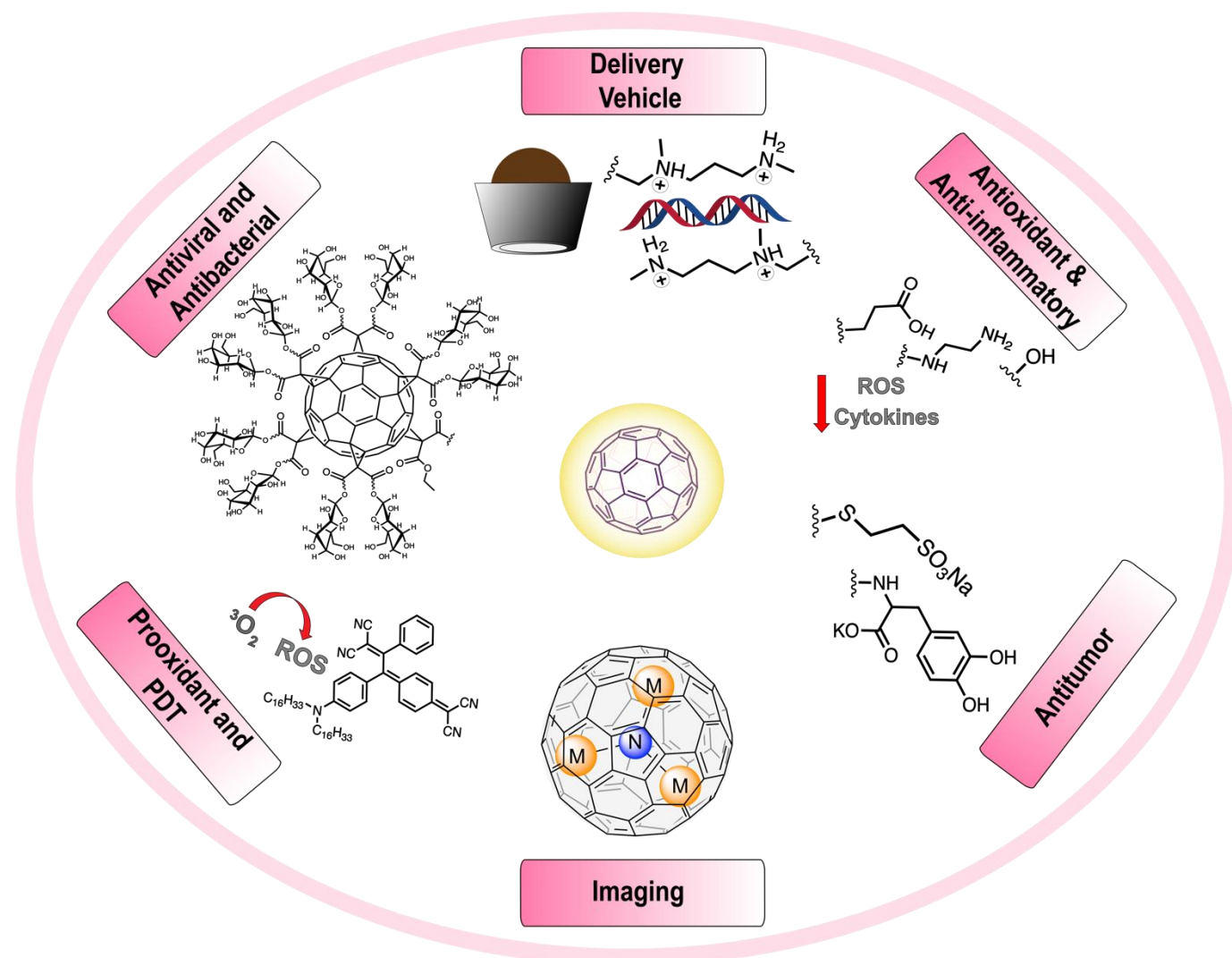


Fig. 1 Various fullerene functionalizations and their biomedical applications. Reproduced from refs. 4-8,10,12,13,16.

Finally, the ability of fullerenes to serve as a host and scaffold towards endohedral and exohedral functionalization, respectively, demonstrated its potential in both diagnostics and therapy. The endohedral encapsulation of metals and metallic clusters,³⁰ such as Gd or Gd₃N, highlights endohedral metallofullerenes (EMFs) as a method for improving the biocompatibility of otherwise toxic yet appealing contrast agents. Additionally, its versatile exohedral functionalization results in a vast ligand space for fullerene conjugation,²⁰ allowing readily modifiable surface properties that can be tuned toward targeting specific cellular conditions.

There are excellent recent reviews focused on the chemistry of fullerenes towards biomedical applications^{19,20} and the application of metallofullerenes for biomedical applications.^{31,32} This review aims to provide a different focus on the biological activity of fullerene materials with an emphasis on the interaction between these materials and the cellular environments.

2. Fullerene trafficking within the cellular space

Optimizing the subcellular trafficking of pharmaceuticals represents an opportunity for greater drug efficacy, namely, reduced dosages and enhanced, localized fluorescent signals.³³ Considering the varied physiochemical environments of the subcellular space, the development of intracellular targeting compounds requires attention to organelle-compatible design.

Plasma membrane

The plasma membrane represents the first area of contact that a pharmaceutical encounters when interacting with a cell. Due to its hydrophobicity, a fullerene cage is expected to interact favorably with the membrane's inner, hydrophobic lipid domain. Hou et al. experimentally investigated the interaction between C₆₀ and a model biological membrane composed of chicken egg phosphatidylcholine (PC) lipid.³⁴ This study utilized unilamellar PC lipid bilayer membranes non-covalently bound onto silica spheres. These solid-supported lipid bilayer membranes (SSLMs) were mixed with aqueous C₆₀ clusters. Removal of the supernatant solution followed by toluene extraction of the membrane-bound C₆₀ from the SSLMs and subsequent

Table 1 Names, structural descriptions, and purity of reported biological fullerenes.

Compound Name Code	Structural Description	Pure Compound ^{a?}	Figure Number	Ref.
JBD-C ₆₀	Mono-pyrrolidine-functionalized C ₆₀ fullerene singly conjugated to a JBD peptide chain	Yes	2	36
C ₆₀ -1, C ₆₀ -2	Mono-pyrrolidine-functionalized C ₆₀ fullerenes with <i>N,N</i> -dimethyl or <i>N</i> -acetyl substitution	Yes	3	38
C ₆₀ -EDA, C ₆₀ -(EDA-EA)	Heterogenous multi-amination of a C ₆₀ fullerene with ethylenediamine-based ligands	No	4	10
FCD	Mono-Bingel C ₆₀ fullerene bearing a PEG chain and cyclodextrin host for DOX	Yes ^b	5	6
hFCD	Heterogenous multi-hydroxylation of FCD	No	5	6
C ₆₀ SNA	Bingel-Hexakis C ₆₀ fullerene connected to 12 DNA strands	Yes	6	68
TPFE	C ₆₀ fullerene functionalized with four amines and an epoxide around a pentagon motif	Yes	7	77
2a-e	Mono-pyrrolidine-functionalized C ₆₀ fullerenes with <i>N,N</i> -dimethyl and various aryl substitutions	Yes	8	24
GF-Ala	Heterogenous multi-hydroxylation and multi-amination of a Gd@C ₈₂ fullerene	No	9	92
C ₆₀ -PEG 1, C ₇₀ -PEG 2, C ₇₀ -PEG 3	Mono-pyrrolidine-functionalized C ₆₀ and C ₇₀ fullerenes bearing <i>N</i> -PEG substitutions	Yes ^b	10	103
14-17	Mono-Bingel C ₆₀ fullerenes connected to glycoconjugated BODIPY structures	Yes	11	105
ZD2-GD ₃ N@C ₈₀	Heterogenous multi-hydroxylation and carboxylation of a Gd ₃ N@C ₈₀ fullerene for peptide conjugation	No	12	122
8b-8e	Hexakis-Bingel C ₆₀ fullerenes connected to two EMFs and ten PEG chains	Yes ^b	13	129

^a Refers to a distinct fullerene derivative with structurally exact functionalization. ^b The PEG ligands may have inherent dispersity.

concentration analysis via HPLC demonstrated that the C₆₀ clusters could accumulate within the hydrophobic lipid domain in a pH-dependent manner. Namely, a higher concentration of membrane bound C₆₀ was observed at lower pH values. These experimental results are further supported by computational investigations by Wong-Ekkabut and co-workers, which demonstrated the spontaneous penetration and localization of fullerene clusters within DPPC and DOPC model bilayers.³⁵ These studies on fullerene clusters and aggregates are especially appropriate given the tendency for fullerene materials to aggregate in aqueous environments.

This general property that the hydrophobic surface of fullerene cages drives its insertion into the plasma membrane has been utilized in the design of membrane-targeted nanoparticles. Nag et al. employed this property in the design of a nanobioconjugate probe for detecting changes in plasma membrane potential.³⁶ The conjugate is built upon a quantum-dot scaffold with outward-extending peptide arms (JBD peptide) capped with terminating C₆₀ cages (JBD-C₆₀, Fig. 2a). The study demonstrated that the JBD peptide arms could insert into biological membranes, as observed by increased alpha-helical stabilization in the presence of a model phospholipid liposomal membrane. To further investigate this membrane-binding, nonconjugated JBD peptides were compared with JBD-C₆₀ conjugates for their affinity to the plasma membrane of A549 cells. Subsequently, through immunoprobings and silver staining, it was found that the JBD-C₆₀ conjugate exhibited significant membrane binding (Fig. 2b). This result highlighted the facilitated membrane accumulation by the hydrophobic surface of the C₆₀. Thus, due to their affinity for the lipid domain, fullerenes represent a potential class of tether molecules for membrane-targeted nanomedicine.

Given the relationship between cell instability and membrane lipid oxidation,³⁷ the plasma membrane represents an area to

attack diseased cells. Shimada and co-workers investigated such membrane-localized ROS generation, and they highlighted a key balance needed between the hydrophobicity and hydrophilicity of fullerene derivatives to maximize its membrane accumulation.³⁸ This work utilized a liposomal membrane-incorporated (LMI) energy donor-acceptor dyad comprising 1,1'-dioctadecyl-3,3,3',3'-tetramethylindodicarbocyanine (DiD) as the donor and C₆₀-1 or C₆₀-2 as the acceptor (Fig. 3a). Accordingly, only when positioned proximally can efficient energy transfer occur between these two components to induce ROS generation (Fig. 3b). The capacity for ¹O₂ generation was monitored for LMIC₆₀-1-DiD or LMIC₆₀-2-DiD, and it was found that LMIC₆₀-1-DiD generated greater ¹O₂ (Fig. 3c). The photodynamic activities of the two fullerene derivatives were

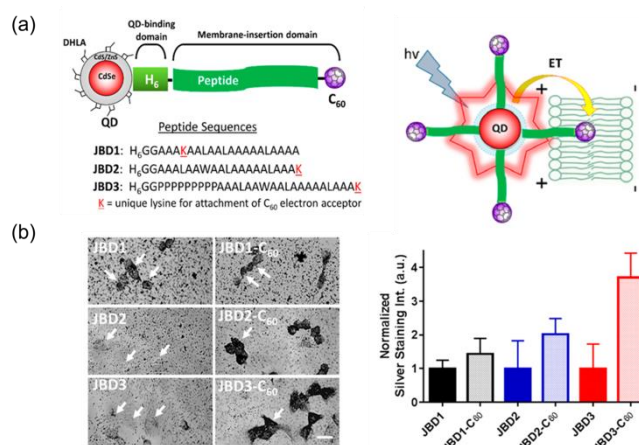


Fig. 2 (a) Design of quantum dot-peptide-C₆₀ bioconjugate and its insertion into the plasma membrane. (b) Micrographs and quantitative measurements of immunoprobings and silver-stained A549 cells after being treated with either nonconjugated JBD-peptide or JBD-C₆₀ conjugate. Scale bar, 20 μm. Reprinted with permission from ref. 36. Copyright 2017 American Chemical Society.

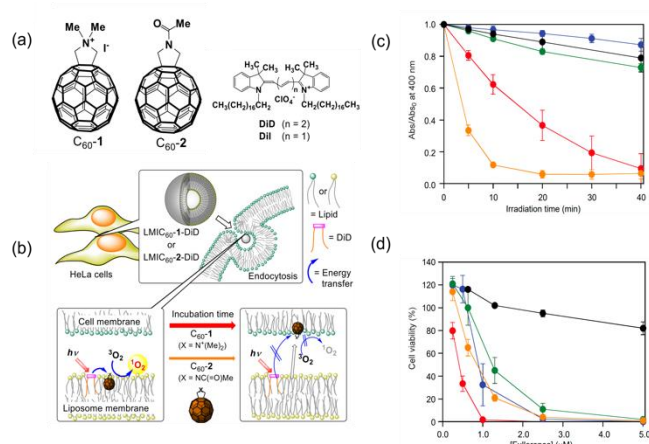


Fig. 3 (a) Structure of fullerene derivatives C_{60} -1, C_{60} -2, and DiD. (b) Schematic of 1O_2 generation activity of LMIC $_{60}$ -1-DiD and LMIC $_{60}$ -2-DiD, their uptake into a HeLa cell, and possible translocation of fullerene derivative from liposomal membrane to HeLa cell membrane. (c) Plot of 1O_2 generating ability of LMIC $_{60}$ -1-DiD (orange) and LMIC $_{60}$ -2-DiD (red) measured by decreases in absorbance. (d) Plot of photodynamic effect of LMIC $_{60}$ -1-DiD (orange) and LMIC $_{60}$ -2-DiD (red) on HeLa cell viability. Reprinted with permission from ref. 38. Copyright 2022 American Chemical Society.

also observed by treating HeLa cell cultures with aqueous solutions of LMIC $_{60}$ -1-DiD or LMIC $_{60}$ -2-DiD. Strikingly, despite the weaker ability to generate singlet oxygen, LMIC $_{60}$ -2-DiD exhibited stronger photodynamic activity toward HeLa cells compared to LMIC $_{60}$ -1-DiD (Fig. 3d). This discrepancy is reasoned as a greater tendency of C_{60} -1 to escape the liposomal membrane and penetrate the neighboring HeLa cell membrane, thus moving away from the DiD energy donor and weakening the energy transfer responsible for the photodynamic activity. The greater liposomal membrane escape is due to the positively charged appendant on C_{60} -1, which may facilitate translocation of the fullerene derivative out of the lipid bilayer. Neutralizing the positive charges, such as in C_{60} -2, reduces the tendency of the translocation and keeps the fullerene derivative localized within the liposomal membrane (Fig. 3b). This membrane anchoring proved significant as LMIC- C_{60} -2-DiD exhibited a photodynamic activity 7.4 times higher than that of photofrin, an established compound utilized in photodynamic therapy.

Such a balance between hydrophilicity and hydrophobicity is further highlighted by the computational work of Kraszewski et al., which demonstrated that increasing the amount of charged appendages would reduce the penetration ability of the fullerene derivative;³⁹ furthermore, neutralizing the charged ligands, such as through proton transfer events can facilitate greater penetration and trafficking of the fullerene within a lipid membrane.

Conjugates that rely on the proximity to the surface of the membrane may benefit from slightly polar appendants. In contrast, conjugates that must be placed nearer to the center of the bilayer may benefit from appendants of lower polarity. Ultimately, the studies presented suggest general considerations toward the design of optimal membrane-targeted fullerenes. Namely, the efficient penetration of a fullerene derivative into the membrane and its subsequent trafficking and localization within the bilayer depends on the cage's hydrophobicity, which

may be tuned through the extent of functionalization and the polarity of the appended ligands.

Cellular Uptake

Fullerene materials can be designed to translocate through the plasma membrane and enter the cytoplasmic space. Similar to other nanoparticles, the uptake of functionalized fullerene materials predominately occurs via endocytic pathways.^{7,40–42} With that said, Lucafo and co-workers had previously reported a fullerene derivative with uptake into MCF7 cells through passive diffusion.⁴³ Given the energy dependence of endocytosis, this conclusion was based on the derivative's significant cell uptake under both physiological and low temperatures. For many other fullerene derivatives, however, endocytosis will predominate.

Ma et al. recently highlighted the importance of surface charge and cellular uptake.¹⁰ Their study involved the use of fullerenes with either a positively charged (C_{60} -EDA) or negatively charged surface (C_{60} -(EDA-EA)) (Fig. 4a). These derivatives were labeled with the organic dye FITC, and their uptake and trafficking were monitored in HUVEC cells. Flow cytometry and Z-stack imaging coupled with confocal microscopy revealed faster cellular uptake of C_{60} -EDA compared to C_{60} -(EDA-EA) (Fig. 4b). The positively charged functional groups were believed to facilitate the binding of C_{60} -EDA to the negatively charged head groups of the plasma membrane, resulting in faster initial uptake. Thus, the presence of basic or acidic groups, which may accumulate charges in the physiological environment, can be utilized to tune the uptake kinetics. Once internalized into the cell, the fullerene will enter an endosomal trafficking pathway. These pathways typically terminate at the lysosomes, though nanoparticles can also escape the endosomes,⁴⁴ thus granting them access to other subcellular domains. Indeed, C_{60} -EDA demonstrated endosomal escape and localized in the mitochondria, whereas C_{60} -(EDA-EA) was found in the lysosomes (Fig. 4c).

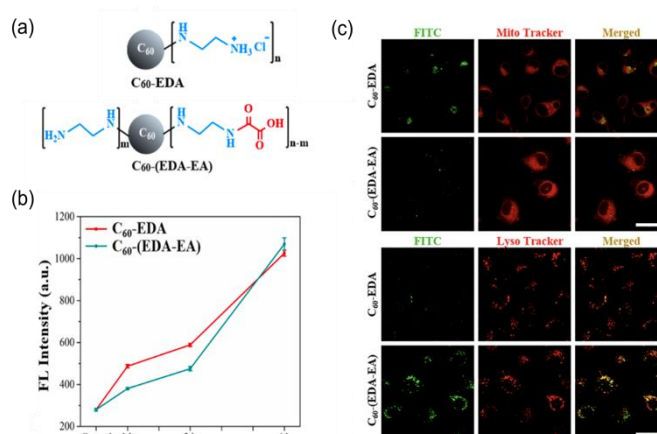


Fig. 4 (a) Structures of fullerene derivatives C_{60} -EDA and C_{60} -(EDA-EA). (b) Quantification of FITC-labelled C_{60} -EDA and C_{60} -(EDA-EA) fluorescence in HUVEC cells via flow cytometry. (c) FL images of HUVEC cells treated with FITC-marked C_{60} -EDA and C_{60} -(EDA-EA) (green) at 50 mg/L for 6 h and costained with MitoTracker (red) and LysoTracker (red). Scale bar, 30 μ m. Reprinted with permission from ref. 10. Copyright 2021 American Chemical Society.

Lysosome

For the fullerene derivatives that remain in the endosomal trafficking pathway, the lysosome is the predominant destination.⁴⁵ Lysosomes are responsible for the breakdown of intracellular material, such as endogenous, damaged proteins, and this breakdown is facilitated by hydrolases and the acidic environment within the organelle.⁴⁶ While these conditions appear harsh, lysosomes are an attractive organelle target. Their acidic environment has been used for pH-sensitive imaging and therapeutic activity.⁴⁷ Additionally, its unique accumulation of enzymes such as β -galactosidase makes the lysosome a relevant target for investigations in senescence and certain cancers.^{48,49}

Li et al. reported the lysosomal accumulation of a bis-malonic acid C_{60} adduct, $C_{60}(C(COOH)_2)_2$, in RH-35 and 3T3-L1 cell lines.⁴¹ The conjugate preserves the cage's conjugation; this system is contrary to fullerene polyglycerol amphiphiles (FPAs), which were reported by Donskyi and coworkers to similarly undergo lysosomal accumulation in A549 cells.⁵⁰ In this work, three different FPAs were studied, each with a different number of polyglycerol branches attached to the cage. The branching difference between the FPAs was within 1–2 branches, thus representing small changes in conjugation. Despite these small changes, all FPAs demonstrated the capability of lysosomal processing.

Towards the end of weak conjugation, fulleranol, $C_{60}(OH)_n$, was reported by Chaudhuri and co-workers to accumulate in the lysosomes of B16-F10 melanoma cells.⁵¹ This work also monitored the subcellular processing of fulleranol in MDA-MB-231 cells, and contrarily, it was shown to have low cellular internalization and lysosomal uptake. Considering that $C_{60}(C(COOH)_2)_2$ contained charged ligands, FPAs contained larger addends, and fulleranol contained small, polar attachments, a diverse set of ligand properties are compatible with lysosomal uptake.

Relatedly, host ligands such as proteins have also been observed to match this compatibility. Di Giosia et al. investigated the intracellular accumulation of lysozyme-encapsulated C_{70} ($C_{70}@lysozyme$).⁵² This system accumulated in the lysosomes of HeLa cells, demonstrating the potential ligand space for optimizing subcellular trafficking.

Nucleus

Upon escape from the endosome, a fullerene derivative may collect within other organelles, such as the nucleus. The nucleus is an appealing subcellular target as it houses the cell's DNA, where damage to it can readily induce cell instability and death.⁵³ We studied the nuclear uptake of two fullerene-based drug delivery systems, Dox@FCD and Dox@hFCD (Fig. 5a).⁶ Dox@hFCD is the hydroxylated variant of Dox@FCD, which was demonstrated to be a significant feature as it allowed for hydrogen-bond driven aggregate formation as opposed to the hydrophobic interaction-induced aggregation in Dox@FCD. Hydrogen-bonded aggregates were shown to be more susceptible to being broken down in acid, which contributed to the greater nuclear localization of Dox@hFCD compared to Dox@FCD in HeLa cell cultures (Fig. 5b,c). Interestingly, the localizations of these two fullerene systems contrast with the lysosomal

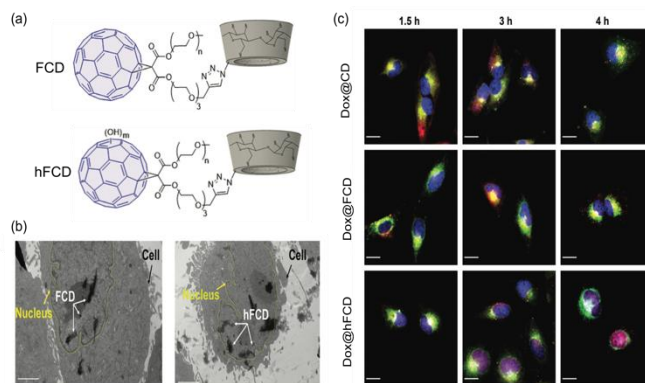


Fig. 5 (a) Structures of fullerene derivatives FCD and hFCD. (b) TEM images of HeLa cells displaying nuclear-localized FCD and hFCD. Scale bar, 2 μ m. (c) Microscope images showing merged fluorescence of DAPI (blue), Dox (red) and LysoTracker Deep Red (green) for Dox@CD, Dox@FCD, Dox@hFCD. Scale bar, 20 μ m. Reprinted with permission from ref. 6. Copyright 2022 The Royal Society of Chemistry.

entrapment of Dox@CD, which lacks a fullerene cage (Fig. 5c). Thus, the addition of the cage appeared to push endocytic escape and nuclear accumulation. Additionally, the hydroxylation further facilitated lysosomal escape and nucleus targeting. Blocking experiment with Thapsigargin showed that the addition of polar functional groups on the fullerene surface enhanced entry into the nucleus via the nuclear pore complex, which is a pathway almost absent in the FCD with a hydrophobic cage.

Importantly, molecularly precise fullerene hexakisadducts have also exhibited nuclear localization. Serda et al. investigated the cellular processing of Sweet- C_{60} , a fullerene-hexakis derivative bearing six glucosamine sugars.¹⁵ The sugars aid the selective uptake of the fullerene into cancer cells, which have an increased demand for glucose. Other fullerene materials have been conjugated to ligands that direct them to specific cells, indicating the applicability of these nanoparticles with cell-specific targeting.^{54,55} Sweet- C_{60} was observed to predominately accumulate in the nuclei of pancreatic stellate cells. The non-fluorescent Sweet- C_{60} was visualized in cells through a fullerene-specific mouse monoclonal antibody. This method of antibody staining, rather than the covalent attachment of a fluorophore, may provide a more accurate idea of the cellular processing as it does not alter the structure of the fullerene material.

Mitochondria

The mitochondria represents another appealing subcellular target, especially since it is directly involved in the energy production of the cell and is also a major source of ROS generation.²⁷ Mono-malonic acid C_{60} , $C_{60}(COOH)_2$, and the tris-malonic acid derivative, $C_{60}(C(COOH)_2)_3$ (C3), were both reported to accumulate within, or associate with, the mitochondria of COS-7 cells and mouse cortical neurons, respectively.^{56,57} Despite the different cell lines used, it is still noteworthy that the mono- and tris-Bingel adducts showed accumulation in the mitochondria while the bis-adduct preferentially localized in the lysosome.⁴¹ This may indicate a nuanced balance between the number of ligands and the total

charge of the molecule, which may shift the preference for fullerene localization.

Relatedly, Wong et al. demonstrated the mitochondrial localization of several fullerene derivatives bearing multiple negatively charged appendants.¹⁶ These findings contrast with the structure-function relationship observed by Ma and co-workers, which involved negatively charged C₆₀-(EDA-EA) localizing in the lysosomes and the positively charged C₆₀-EDA localizing in the mitochondria (Fig. 4c, *vide supra*).¹⁰ While the cells used in the two studies were different, the variation, nonetheless, highlights a complex relationship between surface charge and subcellular fullerene processing that is currently not generalizable.

While the current literature suggests the potential and versatility of fullerene materials in subcellular targeting, the ongoing studies would benefit from two kinds of investigations: (1) elucidation of a structure-function relationship between fullerene design, cellular uptake, and subcellular processing and (2) utilization of less structure-altering methods for monitoring the cellular trafficking. The first investigation is imperative for optimizing nanoparticle design. The second investigation highlights an area of improvement in the current literature, which commonly attaches a fluorescent marker to the nanoparticle through a covalent linkage. This appended fluorophore may introduce enough changes to the fullerene structure to alter its uptake and trafficking properties; consequently, the trafficking of the fluorophore-labelled nanoparticle may not reflect the actual activity of the unlabeled nanoparticle. With that said, the current systems still provide valuable insight for future organelle targeting.

3. Delivery Vehicle

Drug activity is affected by several factors, including aqueous solubility, stability within the physiological environment, rate of metabolism, and cell permeability.⁵⁸ One way to optimize these factors is by attaching the drug to a carrier that can be functionalized to provide desirable properties.^{59,60} In addition to the common advantage of nanoparticle delivery vehicles, fullerenes have the added benefit of molecular precision. Additionally, fullerene materials have been observed to localize in tumor tissue and various cellular compartments,^{10,61,62} allowing for site-directed targeting. Furthermore, these materials can prompt slow drug release and enhance drug exposure to the target site.⁶³ As discussed in this section, fullerenes may also host a variety of ligands, ranging from small molecule therapeutics to larger biopolymers, such as nucleic acids.

Kumar et al. utilized fullerenes as drug-loading scaffolds which were observed to have greater hemocompatibility, higher cytotoxicity towards target cells, and improved pharmacokinetics relative to the free drug.⁶⁴ This work designed the system CF-LYS-TEG-MMF, which consists of a C₆₀ cage decorated with monomethyl fumarate (MMF), an anticancer agent. The cytotoxicity of this system towards SH-SY5Y neuroblastoma cells was investigated, and it displayed an approximately 5-fold increase in toxicity compared to pure MMF. This increased efficacy is suggested to result from more

efficient cell entry of the fullerene nanoconjugate compared to the free drug, leading to a greater concentration of MMF entering cells and subsequently increasing the cytotoxicity of the nanoconjugate drug. Finally, the pharmacokinetics of CF-LYS-TEG-MMF was studied in rodents, and the authors observed a significantly reduced body clearance of the loaded nanoconjugate compared to pure MMF. The moderate zeta potential of the system may have contributed to this lower clearance as a slightly negatively charged nanoparticle surface has been reported to exhibit greater escape from clearance systems such as the reticuloendothelial (RE) or mononuclear phagocytic (MP) systems.¹ Ultimately, the greater penetration of CF-LYS-TEG-MMF and its ability to escape clearance allows the MMF concentration to remain within the therapeutic range at lower dosages.

Relatedly, Chaudhuri et al. investigated the *in vivo* pharmacokinetics of a multi-functionalized C₆₀ cage decorated with hydrophilic PEG groups and doxorubicin (Ful-Dox).⁵¹ The PEGylation of the cage represents a strategic design to bestow water solubility, and it has also been used in other nanoparticle systems to reduce their clearance.¹ The nanoconjugate and free doxorubicin were both injected into mice bearing B16/F10 melanomas. Both treatments resulted in similar attenuated tumor growth; however, the free Dox displayed a lower toxicity threshold as it led to a decrease in mice body weight while Ful-Dox increased body weight. The differential adverse effect was further investigated by probing the biodistribution of Dox and Ful-Dox in the tumor tissue and organs of the mice. Dox displayed undesired accumulation in the spleen and reduced both spleen and heart weight. Conversely, Ful-Dox demonstrated lowered accumulation and toxicities towards the spleen or heart; it also showed greater accumulation into tumor tissue, which may be influenced by the enhanced permeability and retention (EPR) effect, a characteristic of nanoparticles.^{62,65,66} Thus, fullerenes appear to be an appropriate choice as a drug delivery scaffold in chemotherapeutics as it not only reduces toxicity relative to the free drug but also suppresses undesired tissue accumulation and promotes selective tumor targeting.

The molecular precision of fullerenes allows for the controlled incorporation of key nanoparticle design concepts, which can increase accessibility to fundamental interaction investigations.⁶⁷ This advantage is highlighted in a seminal work by Li, Zhang and Mirkin et al. where researchers designed a molecular spherical nucleic acid (SNA) scaffolded onto a C₆₀ fullerene (C₆₀ SNA) (Fig. 6a).⁶⁸ Their system is comprised of a hexakis C₆₀ derivative bearing 12 DNA strands. The controlled multivalent ligand addition led to a monodisperse nanoparticle with a high surface density that offered nuclease resistance (Fig. 6b), which is a retained property of its polydisperse SNA counterparts. Interestingly, the nuclease protection offered by C₆₀ SNA was greater than that of a similarly DNA-functionalized T8 polyoctahedral silsesquioxane nanostructure (POSS SNA). Furthermore, the C₆₀ SNA was observed to undergo significantly greater cellular uptake compared to free DNA and POSS SNA (Fig. 6c), highlighting the utility of fullerenes as a non-viral transfection agent. The transfected fullerene system

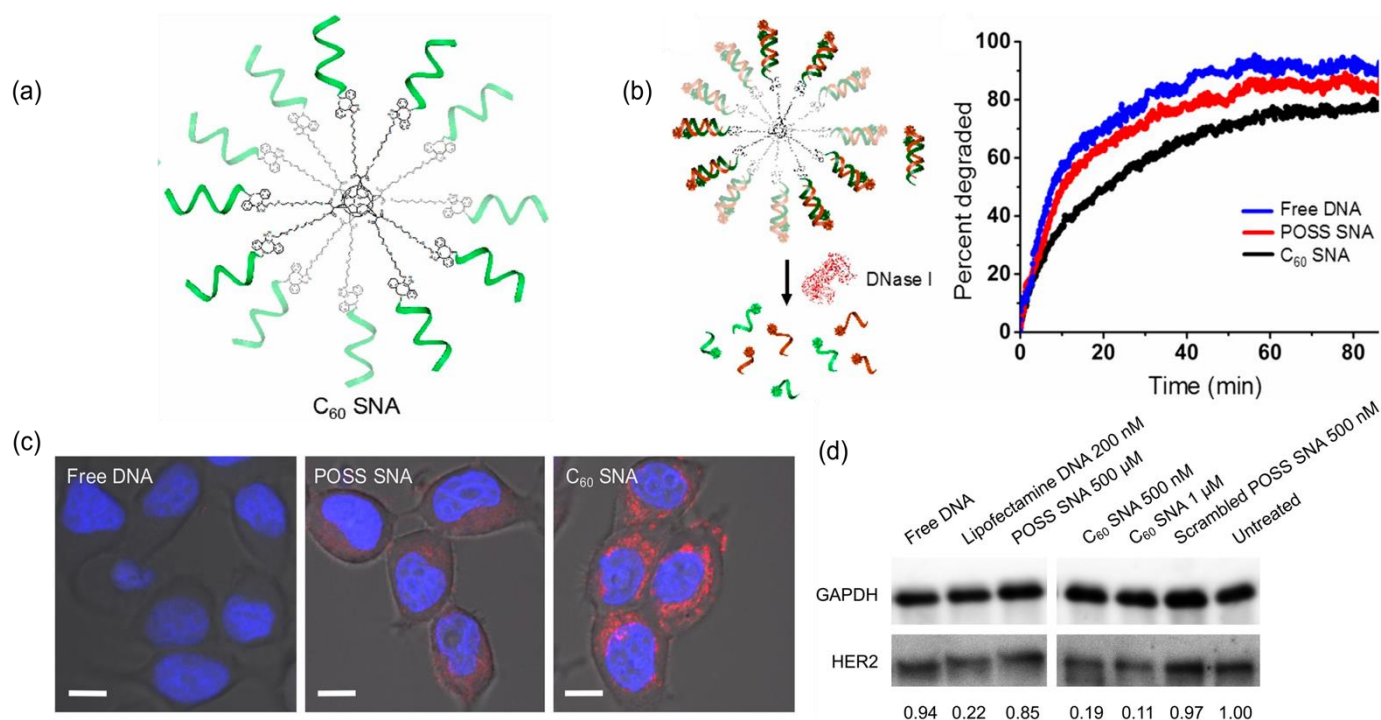


Fig. 6 (a) C₆₀-core SNA. (b) Scheme describing the FRET-based SNA stability assay in the presence of DNase I and percent duplex degraded as a function of time. (c) Cellular uptake of molecular SNAs. Confocal microscopy of MCF7 cells treated with Cy3-labeled free DNA and conjugates (red). Cell nuclei are stained with Hoechst (blue). Scale bar, 10 μm. (d) Western blot analysis of antisense gene silencing efficacy of HER2 using SNAs and controls in SKOV3 cells. Reprinted with permission from ref. 68. Copyright 2018 National Academy of Sciences.

subsequently demonstrated the ability to carry out intracellular gene regulation as evidenced by reduced HER2 expression in SKOV3 cells (Fig. 6d), an ovarian cell line characterized by high HER2 expression. Furthermore, even at lower concentrations, the fullerene-based SNA exhibited superior gene regulation compared to the POSS SNA.

The key researchers of the original molecular SNA work later highlighted the fine structural tuning capability of fullerene materials by designing a similar hexakis system, C₆₀ pacDNA, which contained 1 DNA strand and 11 PEG chains.⁶⁹ The high surface density and steric protection offered by the PEG chains were able to retain the suppressed nuclease digestion found in SNAs and other oligonucleotide-functionalized nanoparticles. The authors also demonstrated the ability to modulate the effective exposed negative charge of their system by orienting the DNA's center of mass closer to the fullerene core. Thus, considering the influence of PEGylation and zeta potential on systemic clearance,¹ this nanoconjugate underscores the potential for precise optimization of its circulation half-life.

In addition to antisense DNA, plasmids have also been stably and effectively delivered into cells through fullerene-based vehicles. Isobe et al. compared the efficacy of a tetraamino fullerene derivative to transfect and protect plasmid DNA in cells.⁷ Chemical experiments probing the endonuclease protection on plasmid DNA illustrated complete suppression of DNA hydrolysis with the tetraamino fullerene while over 50% hydrolysis was observed in a Lipofectin-complexed plasmid. Intracellular experiments also supported greater protection offered by the tetraamino fullerene from lysosomal degradation. Chloroquine is an agent used to suppress the lysosomal

breakdown of DNA, and when treated with the Lipofectin-complexed plasmid, the observed transfection efficiency is comparable to the stability granted by tetraamino fullerene itself. In addition to the plasmid stability, the fullerene-based transfection is more compatible with a variety of cell-culture conditions. Namely, serum is commonly used in cell culture mediums as it supports cell adhesion and proliferation; however, it is typically avoided in cell cultures of cationic lipofectin-based transfections due to its interference with the lipid-DNA complex;^{70,71} accordingly, this work observed a 50% reduction in Lipofectin-based transfection efficiency in COS-1 cells incubated with 10% FBS. In contrast, the tetraamino fullerene system exhibited an increase in transfection under the same cellular conditions. This work also found that their fullerene system was able to transfect 100% confluent COS-1 cells at higher levels than Lipofectin. Ultimately, this tetraamino fullerene-based transfection suggests fullerenes as a potential alternative to commercial Lipofectin agents.

Aside from monodisperse carriers, liposomal-like nanocarriers are sought after in drug delivery for their high drug-loading capacity and modifiable surface;⁷²⁻⁷⁴ however, the hydrophilic interior offered by phospholipid-based liposomes limit their encapsulation to hydrophilic payloads. In response to this limitation, Partha et al. demonstrated the formation of buckysomes, a fullerene aggregate with high compatibility towards hydrophobic drugs. This work utilized a previously reported fullerene derivative AF-1 prompting its supramolecular assembly at the elevated temperature of 70 °C, contrary to the room temperature conditions used in its initial report.^{75,76} This parameter change induced a different structure from the typical

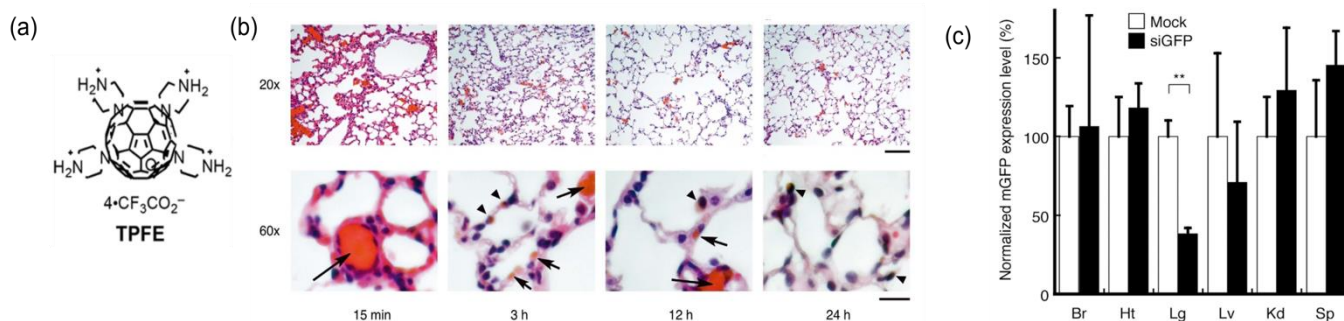


Fig. 7 (a) Structure of TPFE. Reprinted with permission from ref. 77. Copyright 2018 American Chemical Society. (b) In vivo biodistribution of TPFE–siRNA complexes in lung capillaries and cells. Histological appearance of TPFE in mouse lungs sacrificed at 15 min and 3, 12, and 24 h after TPFE–siRNA injection. Hematoxylin and eosin were used as a counterstain. Brownish-orange-colored areas indicate TPFE. Arrows and arrowheads indicate localization of TPFE in the lung capillaries and cells, respectively. Original magnification used and scale bars: (top row), 20 \times and 100 μ m; (bottom row), 60 \times and 20 μ m (c) In vivo biodistribution of injected siRNA in each organ. At 24 h after the injection of TPFE–siRNA complexes, knockdown of mRNA expression of EGFP was detected by real-time RT-PCR. Abbreviations: Br, brain; Ht, heart; Lg, lung; Lv, liver; Kd, kidney; Sp, spleen. (b-c) Reprinted with permission from ref. 78. Copyright 2014 Springer Nature.

vesicular structure; namely, it contained hydrophobic pockets. Subsequently, its therapeutic potential was investigated by loading them with the hydrophobic chemotherapeutic paclitaxel, and the drug-loaded aggregates exhibited similar cytotoxicity as the FDA-approved therapeutic Abraxane towards MCF-7 breast cancer cells.

Minami and co-workers investigated TPFE, an amphiphilic fullerene derivative bearing four piperazine groups (Fig. 7a).⁷⁷ This compound forms a stable micellar structure with an average diameter of 7 nm, and when complexed onto a 21-mer siGFP oligonucleotide, a siRNA that targets enhanced green fluorescent protein (EGFP), the TPFE–siRNA complex forms sub- μ m-sized assemblies. This complex demonstrated further agglomeration with plasma proteins in buffer solution to form a ternary complex of approximately 6 μ m. The size is critical as the diameter of the lung capillaries is only about 5 μ m. Indeed, when the TPFE–siGFP was injected into mice over-expressing EGFP, it complexed with plasma proteins in the blood and became entrapped within the narrow lung capillaries (Fig. 7b).⁷⁸ This clogging resulted in selective and significant gene knockdown in lung tissue of 62% reduction (Fig. 7c). TPFE–siRNA and naked siRNA were also incubated within mouse serum, and the siRNA degradation was measured. While naked siRNA exhibited a 63% degradation in 15 minutes, the TPFE–siRNA system only displayed 22% degradation.⁷⁷ Furthermore, the siRNA delivery of TPFE–siGFP was compared to that of commercial Lipofectamine 2000 in EGFP over-expressing HEK293 cells, and the TPFE–siRNA was found to produce 61% knockdown efficiency, while the commercial lipofection agent produced only 49% knockdown efficiency. Thus, the siRNA delivery is complemented by both the protection offered by PTFE against enzymatic degradation in the serum environment as well as the boost in siRNA delivery offered by the nanoparticle. Although the ternary complex clogging the blood vessel appears problematic, it is loosely held and readily disintegrates after the internalization of siGFP into lung cells. The clogging eventually diminishes, and the small nanometer-sized TPFE assemblies are cleared from the lungs 12 hours post-injection.⁷⁸ Accordingly, this fast clearance from the lungs posed no acute toxicity in vivo,

and it was also demonstrated that the TPFE–siRNA complex posed no cytotoxicity to the HEK293 cells used in the study.

4. Antioxidant & Anti-inflammatory

The oxidative state of a cell is a product of the balance between its antioxidative and pro-oxidative activities that serve to maintain an optimal level of reactive oxygen species (ROS) in the cell.⁷⁹ ROS, such as the hydroxyl radical, superoxide anion, or hydrogen peroxide, are natural byproducts of oxidative metabolism; however, when their levels are disproportionately high, they can react with various biomolecules in the cell, weakening cell integrity and initiating cell death.²⁷ Oxidative stress also appears to be intimately linked with inflammation, as heightened cytokine production can be induced by ROS treatment,⁸⁰ potentially inducing acute inflammation and severe tissue degradation. Given its involvement in a wide array of conditions and pathologies, the restoration of oxidative balance is of paramount importance.

Many fullerene materials are potent antioxidants due to the large number of conjugated double bonds, which can react with radicals; however, the scavenging process may also involve the functional groups on the cage, and the poly-addition of groups such as hydroxyl can also contribute to the high radical quenching ability.^{81,82} Thus, the antioxidant function of a fullerene material may be seen as a balance between the preservation of the cage conjugation and its surface functionalization. Ultimately, investigations attempting to unveil structure–function relationships of fullerenes and their antioxidant activity are important for the future rational design of these nanomaterials.

Aggregation and the morphology of the aggregates represent an important design parameter for antioxidant fullerene derivatives. To this end, the structure–function relationship of oligo(poly(ethylene oxide)) (o-PEO) functionalized C₆₀ derivatives and their ROS scavenging ability was investigated by Chen and co-workers.²⁴ This work synthesized water-soluble derivatives, whose solubility was driven by both the hydrophilic o-PEO chains as well as a cationic center (Compounds 2a–f, Fig. 8a). The derivatives differed in the number of o-PEO chains as

well as their orientation relative to one another. As expected, the increase in the number of hydrophilic chains increased the water-solubility of the derivative, and within groups containing the same chain number, there was an observed dependence of solubility on the positioning of the *o*-PEO ligands on the appended aromatic ring. The effect of these differing structural properties on the aggregation and antioxidant activity of the compounds was further studied. Through various TEM techniques and computational studies applying critical packing parameter (*p*) theory, the morphologies and *p* values of each derivative were investigated (Fig. 8b). For derivatives 2b and 2c, which bear two *o*-PEO chains, compound 2c predominately exhibited nanosheet aggregates. In contrast, compound 2b displayed concentration-dependent polymorphism as a concentration of 100 μM resulted in nanosheet aggregates, whereas an increase to 200 μM resulted in a transition to vesicles. These vesicular aggregates may be described as having greater curvature compared to the nanosheets; thus, the vesicles have a higher amount of the fullerene cage exposed. As the cage is capable of directly reacting with ROS, a greater cage exposure would increase the ROS scavenging and antioxidative function of the derivative. This relationship between curvature and scavenging is supported by their experimental work demonstrating greater scavenging of the hydroxyl radical anion of compound 2b compared to 2c. (Fig. 8c,d,e). In addition to TEM, packing parameter values were calculated for these two derivatives, and the *p* value for compound 2b was lower, indicating a greater cross-sectional area of the hydrophilic portion compared to the hydrophobic part of the aggregate. A similar pattern is observed for derivatives 2d-f, which are functionalized with three *o*-PEO chains. The aggregate morphologies and *p* values were determined. Compound 2d exhibited polymorphism as it showed vesicular, nanorod, and nanotubular structures. In contrast, compounds 2e and 2f both displayed nanowire aggregates. The nanowires exhibited the greatest curvature as well as the lowest *p* values. Subsequently, those derivatives expressed greater ROS scavenging ability compared to derivative 2d (Fig. 8c,d,e). Overall, the more water-soluble derivatives aggregated into structures with greater curvature, cage exposure, and ROS scavenging ability.

Since the fullerene cage is hydrophobic, it may readily interact with hydrophobic protein pockets through dispersion forces and π - π stacking interactions; similarly, functionalization of the cage with polar groups may still allow fullerene-protein binding via hydrogen bonding and salt bridge formation.^{83,84} Roy et al.⁸⁵ investigated the binding of C_{60} and its polyhydroxylated variant, fulleranol, towards ribonuclease A (RNase A), and the antioxidative protection offered by these nanoparticles under oxidative stress. Through both experimental and computational studies, C_{60} was found to bind primarily to aromatic and non-polar residues, while fulleranol bound primarily to polar residues. C_{60} also seemed to bind at strictly allosteric sites on RNase A, while fulleranol showed binding to both allosteric and active sites. The placement of the enzyme under oxidative stress promotes an RNase dimer to form.⁸⁶ Pre-treatment of the enzyme with either C_{60} or fulleranol demonstrated reduced dimer formation, with fulleranol showing greater reduction at lower

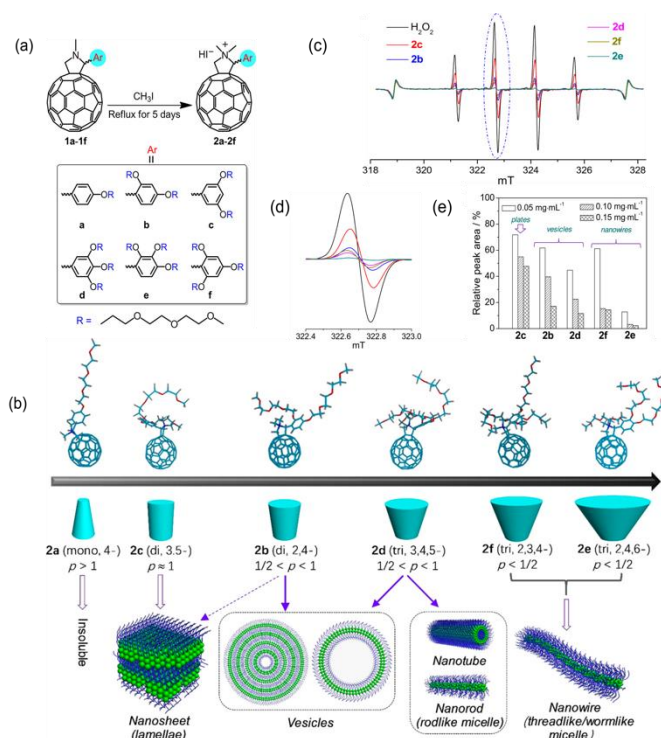


Fig. 8 (a) Structures of the neutral (1a–1f) and ionic (2a–2f) C_{60} derivatives and illustration of the quaternization from 1a–1f to 2a–2f. (b) Structures of 2a–2f optimized in vacuum and illustration of their aggregation behavior in water governed by the critical packing parameter *p*. (c) ESR spectra of 250 $\mu\text{mol}\cdot\text{L}^{-1}$ H_2O_2 aqueous solution at the presence of 0.15 $\text{mg}\cdot\text{mL}^{-1}$ 2b–2f. (d) Magnified spectra in the range of 322.4–323.0 mT (the peak indicated by the ellipse in c). (e) Relative peak area at varying concentrations of 2b–2f. Reprinted with permission from ref. 24. Copyright 2019 American Chemical Society.

concentrations. However, fulleranol exhibited a hormetic effect as concentrations above 10 $\mu\text{g}/\text{mL}$ increased dimer presence, indicating increased oxidation and highlighting the importance of maintaining an optimal level of the antioxidant system.²⁷

Previous work with C_{70} @lysozyme and C_{60} @lysozyme highlighted the single-molecule dispersion offered by the lysozyme host.^{52,87} Such dispersion is important as aggregation has been shown to impact the exposed surface area available for radical scavenging.²⁴ Furthermore, the utilization of a protein host would prevent the need for further tampering with the fullerene derivative's structure for bestowing water solubility. Thus, these recent works encourage the advantageous use of protein-based hosts as carriers for both hydrophilic and hydrophobic fullerene materials in oxidative stress environments.

In addition to the *o*-PEO functionalized derivatives and fulleranol, many other fullerene materials exhibit potent antioxidant activity, such as carboxylated fullerene, aminated fullerene, and EMFs, such as gadofullerene.^{10,12,88–90} Gadofullerenes have demonstrated higher electron affinities compared to their empty cage counterparts, resulting in a greater reactivity towards radical species.⁹¹ Thus, gadofullerenes have been a powerful choice of scaffold for ameliorating oxidative-stress-induced damages. An important work by Zhou, Wang and Bai et al. sought this increased antioxidative property in GF-Ala, a β -alanine-decorated gadofullerene (Fig. 9a).⁹² The effect of

this ROS-quenching ability was tested on oleic acid-treated L02 cells and a hepatic steatosis ob/ob mouse model, which is characterized by the build-up of hepatic lipids, increased oxidative metabolic rates, and oxidative stress,⁹³ which can trigger a positive feedback mechanism that potentiates its damage.⁹⁴ In cells, it was shown that GF-Ala restored proper mitochondrial function as properties such as mitochondrial membrane potential, which was decreased, and complex I activity, which was over-stimulated, were restored to more optimal levels after GF-Ala treatment. ROS levels in the L02 cell model were also diminished with GF-Ala, as observed by DCF fluorescence. (Fig. 9b). This decrease in oxidative stress was further accompanied by a reduction in lipid peroxidation in L02 cells, as evidenced by lower malondialdehyde levels. A balance in ROS and reduction in lipid peroxidation inhibits the degradation of triglyceride transport protein ApoB100, allowing it to transport excess TGA out of the cell. Accordingly, the levels of ApoB100 were compared between control and treatment mice via quantitative proteomics and western blot analysis. It was found that ApoB100 protein levels were decreased in control ob/ob mice; however, those levels were elevated under GF-Ala treatment. Consequently, compared to control mice, ob/ob mice

treated with GF-Ala for 15 days exhibited a reversal of hepatomegaly and a reduction in the hepatic neutral lipid content and hepatic free fatty acid content (Fig. 9c,d). Thus, the antioxidative capacity of fullerenes exhibits a pleiotropic effect ranging in relief from oxidative stress, reduced lipid accumulation, restoration of mitochondrial function, and inhibition of protein degradation.

In addition to protection against oxidative stress, many fullerene materials exhibit anti-inflammatory functions and have been used to ameliorate many chronic inflammatory disease models. Zhou et al. investigated such anti-inflammatory properties of polyhydroxylated Gd@C₈₂ (GF-OH) and C₇₀ (C₇₀-OH) in a pulmonary fibrosis mouse model.⁹⁵ When injected into fibrotic mice, GF-OH and C₇₀-OH improved alveoli integrity, suppressed collagen deposition, and mitigated fibrosis relative to mice treated with only saline. The expression of TGF- β 1, an inflammatory cytokine,⁹⁶ was also investigated, and it was found to be reduced under GF-OH and C₇₀-OH treatment, representing their action against early inflammation regulation.⁹⁵

Among fullerene derivatives, fulleranol is the most prominently investigated due to its ease of synthesis, high water solubility, and potent radical scavenging and anti-inflammatory

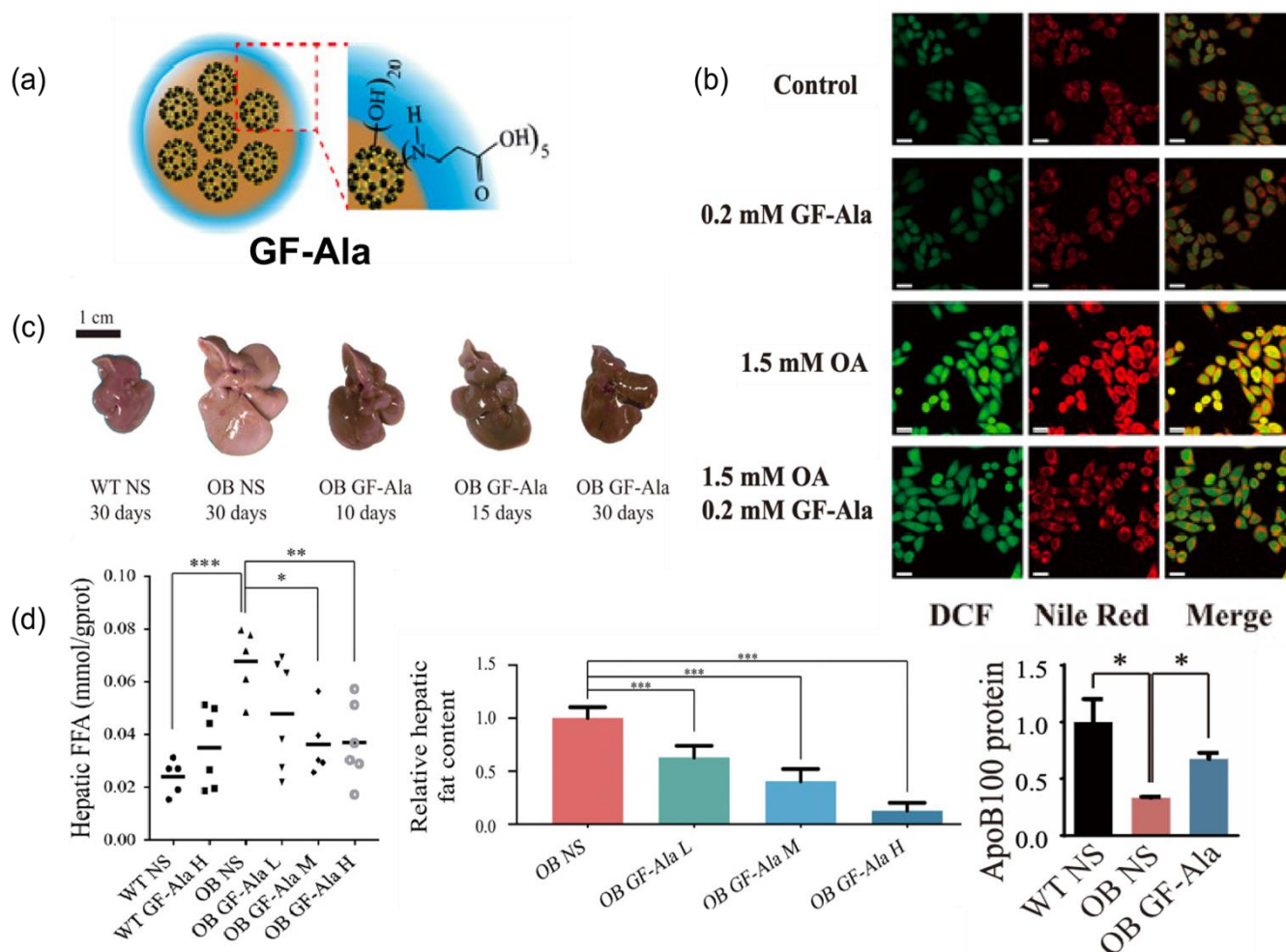


Fig. 9 (a) Schematic of GF-Ala structure. (b) Confocal fluorescence images of ROS (DCF) and lipid (Nile Red) in L02 cells incubated with OA, GF-Ala, or together. Scale bars, 50 μ m. (c) Photographs of liver tissues after sacrificing by GF-Ala treatment with different therapeutic periods. (d) Levels of hepatic FFA, hepatic fat content, and protein expression of ApoB after GF-Ala treatment (L, low; M, medium; and H, high). Reprinted with permission from ref. 92. Copyright 2020 American Association for the Advancement of Science.

functions; consequently, it has been used as a therapeutic in several disease models.^{28,89,97–99} Xiao et al. highlighted the therapeutic utility of fullerene in a lumbar radiculopathy mouse model, and it was shown that compared to untreated mice, the fullerene-administered mice exhibited decreased sensitivity to pain, which normally results from an accumulation of nociceptive factors in response to inflammatory signaling. These pleiotropic anti-inflammatory effects in response to TNF- α stimulation were found for several other fullerene derivatives under various stimuli, including LPS- and H₂O₂-induced inflammation.^{12,90}

Derivatives such as fullerene or polyaminated fullerene are widely studied; however, they lack specificity toward a target tissue, thus requiring the direct administration of these materials at the infected site.²⁸ This limitation has encouraged investigations into target-specific fullerene derivatives. One such system, proposed by Xiao et al., is based on a carboxylated fullerene bearing a peptide that can specifically bind towards formyl peptide receptor-1, which is upregulated in activated macrophages and other leukocytes during inflammation.⁸⁹ This nanoparticle system (FT-C₆₀) demonstrated preferential binding to LPS-stimulated macrophages *in-vitro*. Similarly, intravenous injection of FT-C₆₀ into the tail veins of a lumbar radiculopathy mouse model also exhibited favored accumulation at the disc injury site. The *in vivo* accumulation is consistent with the inflammatory infiltration into the disc during herniation. The anti-inflammatory property of FT-C₆₀ was investigated in LPS-stimulated macrophages. The nanoparticle demonstrated strongly reduced mRNA expression of various inflammatory cytokines, including IL-6, TNF- α , IL-1, and COX-2. These protective cellular effects translated to its analgesic property, whereby a single dosage of FT-C₆₀ (10 nmol/20 g mice) decreased pain sensitivity in disc-herniated mice, persisting up to 12 days post-administration. Thus, FT-C₆₀ not only improves the specificity of fullerene materials but also illustrates clinical benefits as it displays potent anti-inflammatory properties.

5. Pro-oxidant

In contrast to its antioxidative property, interestingly, fullerenes also exhibit pro-oxidative activity, namely, through the production of ROS. This ROS-generating ability may be observed in cells without light;^{16,100} however, it is typically observed under irradiation.¹⁰¹ Such light-induced ROS generation is taken advantage of in photodynamic therapy (PDT), bestowing both spatial and temporal control during the treatment.¹⁰² PDT involves the irradiation of a photosensitizer at an appropriate wavelength to generate ROS in a desired region of the body. The photosensitizer is a molecule that can undergo efficient intersystem crossing (ISC) after excitation, and the generated triplet-excited state can then react with triplet oxygen and convert it to cytotoxic ROS through two mechanistic pathways: the type I pathway, which involves electron transfer and produces O₂^{•-}, and the type II pathway, which involves energy transfer and produces ¹O₂ (Fig. 10a).^{26,103} Another key feature of the photosensitizer is the absorption of visible to near-infrared (NIR) light, which avoids the higher cytotoxicity and

lower tissue penetration associated with shorter wavelength light. Fullerene materials represent promising PDT photosensitizers as it shows very efficient ISC that is conserved in a variety of fullerene derivatives.²⁶ Furthermore, while the bare fullerene cage shows weak absorption in the Vis-NIR region,³ it can be functionalized with chromophores to form dyads that participate in chromophore-to-fullerene energy transfer. Accordingly, the development of efficient photosensitizers requires attention to several parameters such as absorption wavelength, absorption intensity, triplet state population, triplet state lifetime, and mechanism of ROS generation (type I or type II).

Liu et al. highlighted the effect of structure on photodynamic activity.¹⁰⁴ This work investigated the di-, tri-, and quadri-malonic acid derivatives of C₆₀ and C₇₀. While all six derivatives displayed negligible dark cytotoxicity, they significantly reduced HeLa cell viability upon irradiation with white light. The C₇₀ derivatives outperformed their C₆₀ counterparts, which is consistent with the higher absorption of C₇₀ in the visible range. Additionally, in both C₆₀ and C₇₀, the tri-malonic acid derivative demonstrated a higher inhibitory effect compared to the di- or quadri-malonic acid variants. The ROS generation of the tri-malonic acid C₇₀ derivative was also investigated, and the derivative was found to induce cell death mainly via type II ¹O₂ generation. Ultimately, these results underscore the influence of cage structure and level of functionalization for optimizing the photodynamic activity of fullerene materials.

The mechanism of ROS generation may be particularly important when considering the subcellular localization of a fullerene derivative. Namely, if a derivative is designed to target an area with a high concentration of electron donors, such as within the electron transport chain of the mitochondria, then it would be ideal to design a fullerene material with a tendency to undergo type I ROS generation, which requires a reducing agent. Liosi et al. offered crucial insight into the structure-property relationship of C₆₀ and C₇₀ derivatives (C₆₀-PEG 1, C₇₀-PEG 2, C₇₀-PEG 3) and their favored mechanism of ROS generation with a somewhat surprising finding (Fig. 10b).¹⁰³ The PEG ligands were the same across the three compounds; however, the two C₇₀ derivatives differed in their regiochemistry. ESR measurements of stable spin traps were performed to probe the type II ROS generation upon 528 nm irradiation, and it was found that C₇₀-PEG 2 exhibited the highest ¹O₂ generation (Fig. 10c). Similar ESR measurements were performed to probe ROS generation via the type I pathway; namely, the spin trap experiment with or without L-histidine, which inhibits the O₂^{•-} generation via an extension of the type II pathway (Fig. 10a). C₆₀-PEG 1 and C₇₀-PEG 3 illustrated higher O₂^{•-} generation compared to C₇₀-PEG 2. In addition, L-histidine significantly reduced the O₂^{•-} formation from C₇₀-PEG 2, indicating a strong type II pathway to generate its ROS (Fig. 10c). In contrast, C₆₀-PEG 1 and C₇₀-PEG 3 demonstrated similar ROS generation with or without L-histidine, indicating their preference for the type I pathway. Laser flash photolysis was performed, and among the three derivatives, C₇₀-PEG 2 displayed the longest triplet-state lifetime of 7 μ s alongside the shortest triplet-state decay rate constants (Fig. 10b). In addition, the reduction rates

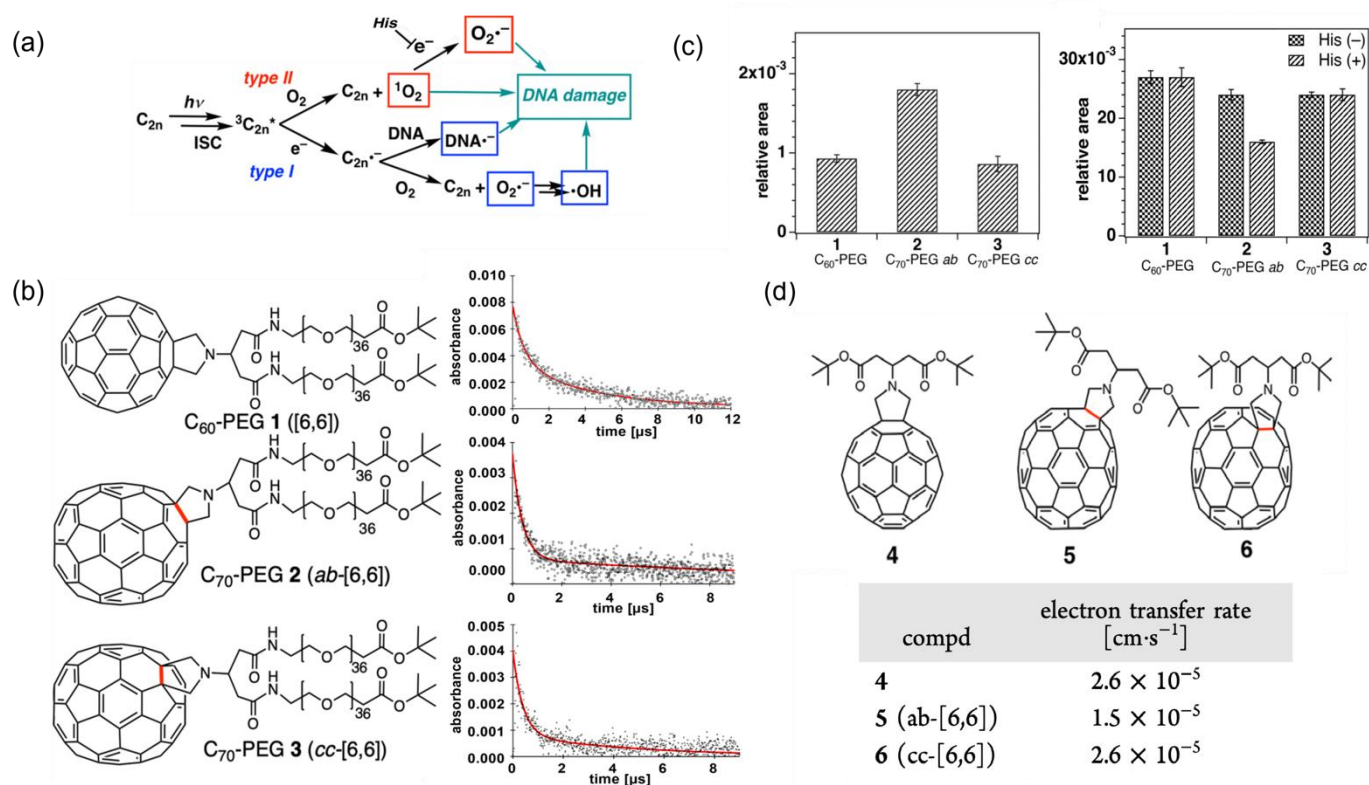


Fig. 10 (a) Diagram depicting photoinduced reactive oxygen species generation from fullerenes and expected pathways for DNA damage. (b) Structures of C₆₀-PEG 1 and C₇₀-PEG 2-3 conjugates and their corresponding laser flash photolysis in water with double exponential fit for the decay of the excited states (c) (Left) Relative amount of ¹O₂ generation estimated by double integration of the ESR signals. (Right) Relative amount of O₂^{-•} generation estimated by double integration of ESR signals in the absence and presence of L-histidine. (d) Structures of Prato adducts 4, 5, and 6, which are precursors to C₆₀-PEG 1, C₇₀-PEG 2, and C₇₀-PEG 3, respectively and their corresponding electron transfer rates. Reprinted with permission from ref. 103. Copyright 2021 American Chemical Society.

of the synthetic precursors to the three derivatives were investigated. These precursor studies suggested that C₆₀-PEG 1 and C₇₀-PEG 3 have faster reduction rates compared to C₇₀-PEG 2 (Fig. 10d). Thus, the type II preference of C₇₀-PEG 2 is rationalized by its long-lasting triplet state and slow rate of reduction, which allow for increased interactions between itself and ³O₂ and suppress the competing type I pathway. In contrast, C₆₀-PEG 1 and C₇₀-PEG 3 were characterized by quicker reduction rates, allowing for increased entrance into the type I pathway and, ultimately, increased O₂^{-•} generation.

In the previous examples, the C₆₀ fullerene derivative displayed very weak absorbance intensity in the visible region. In ideal PDT photosensitizers, the system should absorb visible light to avoid the penetration limitations and cytotoxicity of shorter wavelength light. To circumvent its poor absorption,³ C₆₀ has been modified with a chromophore.²⁶ After chromophore excitation, efficient energy transfer is observed from it to the fullerene cage, promoting the cage into an excited state and allowing it to undergo ISC and generate ROS. Relatedly, Gündüz et al. designed energy donor-acceptor dyads **14-17** that consist of a glucose-functionalized BODIPY energy donor and a C₆₀ energy acceptor (Fig. 11a).¹⁰⁵ The BODIPY moieties exhibited absorbance maxima around 640 nm, and they displayed little change in absorbance after attachment to the C₆₀ cage. However, the fluorescent quantum yields of the BODIPY-fullerene dyads were less than 1%, indicating efficient energy transfer from the excited BODIPY to the cage (Fig. 11b). Subsequently, the

authors confirmed the ¹O₂-generating ability of the BODIPY-fullerene dyads based on decreased DPBF absorbance intensity upon irradiation with 630 nm light (Fig. 11c). Interestingly, dyads **15** and **17**, with two equivalents of BODIPY, expressed lower singlet oxygen quantum yields than the 1:1 counterpart **14**. While it is proposed that such a decrease may be due to energy loss from backward energy transfer from fullerene to BODIPY, other reported BODIPY-fullerene dyads show higher singlet oxygen quantum yields in the derivatives containing two BODIPY equivalents;¹⁰⁶ thus, further studies elucidating the interactions of multiple energy donors with the fullerene cage would be important. ROS generation in K562 cells was also investigated via MTT assay, and the cells showed decreased cell viability after incubation with the dyads and 660 nm irradiation for 8 hours. No cytotoxicity under dark conditions, but upon irradiation, dyads **14**, **15**, **16**, and **17** gave IC₅₀ values of 9.34, 7.70, 9.21, and 10.29 μM, respectively (Fig. 11d). Accordingly, these results demonstrate the potent activity of these BODIPY-fullerene systems and their ideal properties, such as long-wavelength excitation and negligible inherent cytotoxicity. Ultimately, this work highlights the advantage of fullerene derivatives as photosensitizing materials, which draws from its robust and efficient ISC, permitting a range of functionalization while still allowing high triplet-state formation upon excitation. Such a property is lacking in many other photosensitizer designs, such as those that depend on heavy atoms.²⁶

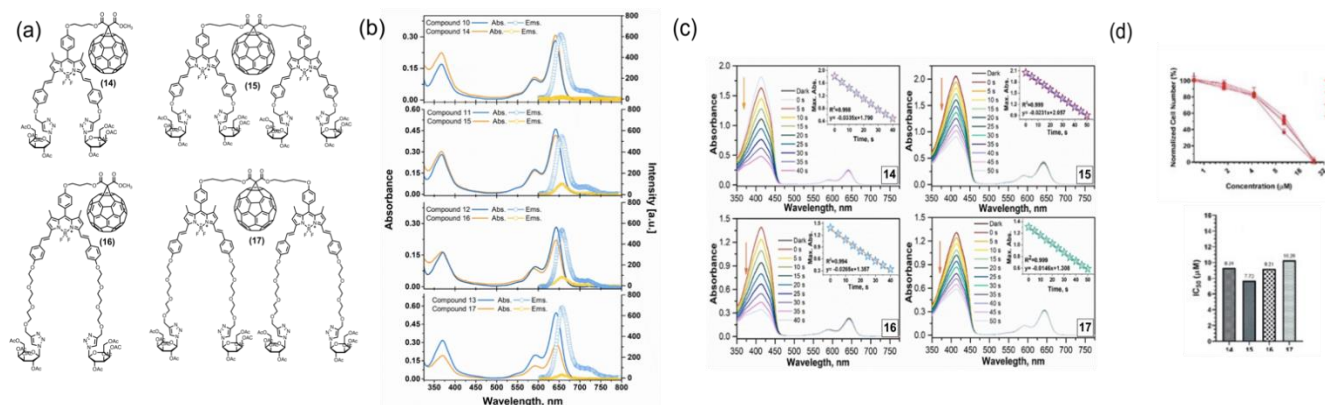


Fig. 11 (a) Molecular structures of the amphiphilic BODIPY-fullerene systems. (b) Absorption and fluorescence spectra of BODIPY-containing systems (2 μM , $\lambda_{\text{exc}} = 590 \text{ nm}$). (c) Singlet oxygen generation of compounds **14**, **15**, **16**, and **17** in DCM (2 μM). (d) The effects of **14–17** on K562 cancer cells and their corresponding IC_{50} values. Reprinted with permission from ref. 105. Copyright 2021 John Wiley and Sons.

For PDT, the chromophore needs to be in close proximity to the cage to maximize the energy transfer and ROS generation; this close association results in quenched fluorescence of the attached chromophore^{107,108} and limits opportunities for fluorescent phototheranostic fullerene systems. Such theranostic systems have been heavily investigated for their potential use in image-guided precision medicine.^{109,110} Accordingly, while fluorescence imaging may be difficult to realize, optoacoustic (OA) imaging is readily achieved and is very compatible with the fullerene cage due to its tendency to undergo non-radiative relaxation.^{52,111} Shi et al. demonstrated such a system by designing DAF-NP, a fullerene-based nanoparticle capable of OA imaging and PDT.¹³ DAF-NPs showed strong absorption in the NIR region, allowing for deep-tissue ROS generation. Within HeLa cell-bearing mice, the OA contrast of this system was localized at the tumor site: a product of the fullerene's established EPR.⁶² Ultimately, the non-radiative decay of fullerenes offers advantageous properties at the level of ROS generation and OA imaging, holding them as promising materials for image-guided phototherapies. Investigations have been made, however, towards fluorescent phototheranostic fullerene systems. Tang et al. designed such a system consisting of a C₆₀ cage functionalized with rhodamine B (C₆₀-RB), a pH-responsive dye.¹⁴ Fluorescence measurements of C₆₀-RB in acidic medium indicated strong quenching due to the cage, resulting in a fluorescence quantum yield of 0.026. Accordingly, in vitro experiments in acidic solution and in cells indicated strong singlet oxygen generation of C₆₀-RB within HCT-116 cells. Explicably, via confocal microscopy, C₆₀-RB was shown to localize in the lysosomes of several cell lines as well as exhibit notable fluorescence signals despite its strongly quenched fluorescence.

Interestingly, Kwag et al. synthesized a hyaluronated fullerene polymer that did not involve attachment of a fluorophore; yet, it still demonstrated greater absorption and fluorescence above 600 nm relative to unmodified C₆₀.⁵⁴ Studies in solution, tumor cells, and tumor-bearing mice showed significant ROS generation and phototoxicity of the hyaluronated fullerene upon irradiation with 670 nm light. Its utility in fluorescence imaging was also investigated in vivo. Hyaluronated fullerene was injected intravenously into CD44+

HCT-116 tumor-bearing mice, and in a time-dependent manner, a tumor-localized fluorescence signal was observed to increase in intensity. This localization may be attributed to both the EPR effect as well as the affinity of hyaluronic acid towards the CD44 receptor, which is upregulated in many tumors.¹¹² Ultimately, this study presents the possibility of a fullerene-based phototheranostic that lacks a fluorophore.

While the pro-oxidative property of fullerenes is mainly manifested via irradiation, some works have demonstrated ROS-generation in dark conditions. Wong et al. investigated the antitumor activities of several water-soluble fullerene derivatives.¹⁶ Of these derivatives, a multi-sulfonated fullerene displayed the greatest cytotoxic activity towards A549 cells, a cancerous cell line, whereas no cytotoxicity was observed in normal bovine endothelial cells. Further investigation of the cellular activity of this sulfonated fullerene revealed an increased cellular oxidation occurrence in fullerene-treated A549 cells compared to untreated cells, indicating upregulated ROS production. The sulfonated fullerene also resulted in a modest impairment of mitochondrial function, which could have contributed to the ROS generation; however, a separate fullerene derivative tested in this study prompted stronger mitochondrial dysfunction yet did not display the same significant ROS-generating ability. Thus, the ROS-generating mechanism of this system remains unclear. Nevertheless, the work demonstrated possible pro-oxidative property associated with the sulfonated fullerene derivative, and the elucidation of this property, as well as its selectivity towards tumor cells, would support the optimized design of other inherently pro-oxidative fullerene materials.

Yang et al. discovered a bis-methanophosphonate fullerene (BMPF) that exhibited pro-oxidative activity towards human disc cells.¹⁰⁰ When human annulus fibrosis and nucleus pulposus cells were cultured with BMPF, there was a dose-dependent decrease in the mRNA levels of aggrecan, type I collagen, and type II collagen. In contrast, BMPF induced an increase in gene expression of matrix metalloproteinase-3, an enzyme involved in the degradation of proteins in the extracellular matrix. Thus, this fullerene derivative takes part in disc degeneration. To test for ROS-based activity, annulus fibrosis cells were incubated with BMPF and ascorbic acid, an established ROS scavenger, and it

was found that the changes in mRNA production induced by fullerene derivative were attenuated by ascorbic acid. Thus, BMPF may be generating ROS within disc cells and, subsequently, causing damage to proteins involved in regulating the expression of intervertebral disc-related genes.

6. Endohedral Metallofullerenes

Fullerenes are hollow cages that are capable of encapsulating atoms and metal clusters.³² Notably, the encapsulation of these guests is very robust such that there is no escape of the contained species. This property allows for the encapsulation of toxic heavy metals without the risk of their leakage into the biological medium. The leakage of gadolinium, for instance, in current commercial MRI contrast agents pose safety concerns of increased risk for nephrogenic systemic fibrosis (NSF) and Gd accumulation in the brain,^{113–115} inspiring many investigations on ways to suppress this metal leakage.¹¹⁶ Thus, Gd EMFs represent an ideal platform for an MRI contrast agent that aims to be biocompatible while utilizing the appealing contrast properties of the toxic Gd metal.

In addition to metal encapsulation, the surface functional groups promote proton exchange with water, and induce aggregation of EMFs into large (~100 nm) ensembles¹¹⁷ which bestows high rotational correlation time. These factors give them remarkable T_1 relaxivity values ($60\text{--}200\text{ mM}^{-1}\text{s}^{-1}$)^{118,119} compared to commercial contrast agents ($4\text{--}10\text{ mM}^{-1}\text{s}^{-1}$).¹²⁰

Such contrast enhancement directly leads to imaging sensitivity that is otherwise very difficult to achieve with small-molecule Gd-based contrast agents (GBCAs). For example, a polyhydroxylated Gd@C₈₂ EMF displayed enough contrast enhancement to detect early-stage tumors of 0.5 mm in diameter.¹²¹ The contrast enhancement is nicely covered in

another review.³² Notably in Section 4 we have cited examples of using gadofullerenes for anti-oxidants, which are expected to have higher efficiency than C₆₀ counterparts; with that said, GBCAs is a direction that Gd EMFs make a fundamental difference and their characters cannot be mimicked by any other type of materials. In this section, we focus on recent work that can transition functional EMFs into feasible GBCAs.

Gd-based EMFs can be functionalized with targeting moieties to enhance the localization of the contrast signals. Han et al. tagged a water-soluble Gd₃N@C₈₀ with a ZD2 peptide (ZD2-Gd₃N@C₈₀) that can selectively bind to extracellular matrix fibronectin (EDB-FN), an extracellular protein overexpressed in aggressive forms of cancer (Fig. 12a).¹²² Thus, EDB-FN can be used to differentiate between high-risk, aggressive cancers from lower-risk non-metastatic cancers, which can enable early characterization of an aggressively developing tumor. The measured r_1 value of ZD2-Gd₃N@C₈₀ at 1.5 T was $223.8\text{ mM}^{-1}\text{s}^{-1}$, which was higher than that measured for the Gd₃N@C₈₀ metallofullerenol synthesized in this study (Fig. 12b) and also considerably higher relative to commercial agents at the same field strength.¹²⁰ Two separate mice models of MDA-MB-231 and MCF-7 tumor-bearing mice were utilized in this study to represent an aggressive triple-negative breast cancer (TNBC) and low-risk breast cancer, respectively. ZD2-Gd₃N@C₈₀ and Gd₃N@C₈₀ metallofullerenol were injected intravenously, and contrast enhancement at the tumor site was monitored up to 30 min post-injection. ZD2-Gd₃N@C₈₀ exhibited strong contrast enhancement in MDA-MB-231 mice; whereas it showed little signal accumulation in the MCF-7 mice, indicating its ability to discern between the high-risk TNBC and the lower risk cancer. Furthermore, ZD2-Gd₃N@C₈₀ showed greater contrast in MDA-MB-231 mice compared to Gd₃N@C₈₀ metallofullerenol, highlighting the targeting effect bestowed by the ZD2 peptide.

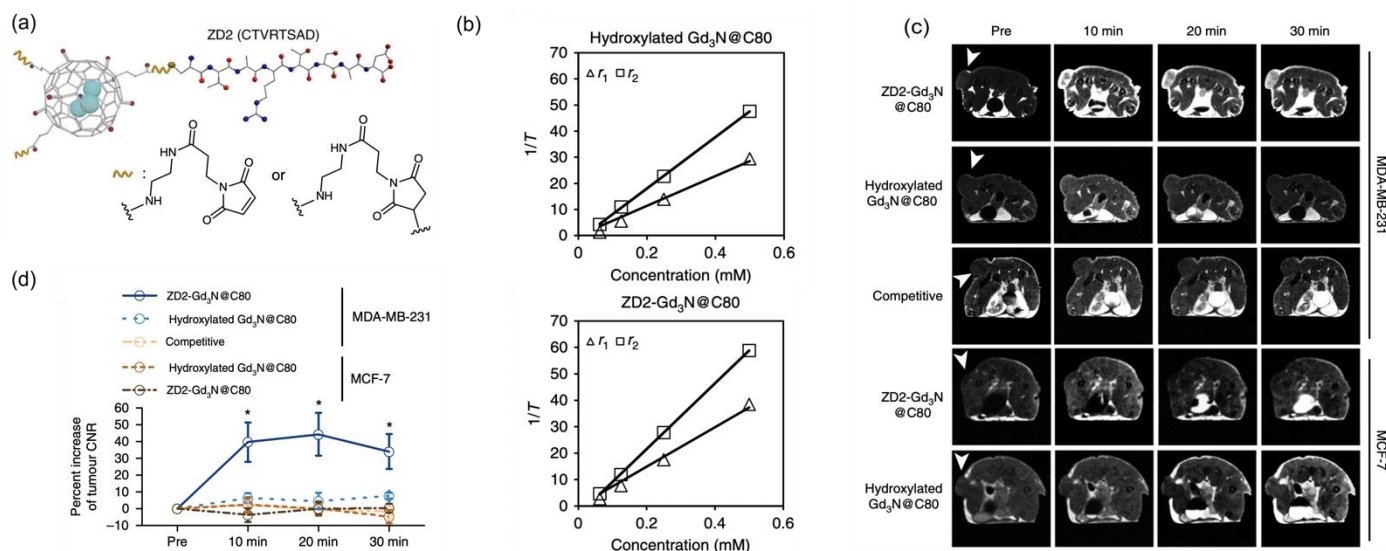


Fig. 12 (a) Structure of ZD2-Gd₃N@C₈₀. Cyan, Gd; blue, nitrogen; red, oxygen; grey, hydrogen. (b) Plots of $1/T_1$ and $1/T_2$ vs. contrast agent concentrations for calculation of r_1 and r_2 relaxivities of hydroxylated Gd₃N@C₈₀ and ZD2-Gd₃N@C₈₀ at 1.5 Tesla. (c) Contrast enhanced MRI with ZD2-Gd₃N@C₈₀ of MDA-MB-231 and MCF-7 tumors in mice. Representative axial T_1 -weighted 2D spin-echo MRI images of MDA-MB-231 and MCF-7 tumors in mice. Images were acquired before and at 10, 20 and 30 min after injection of ZD2-Gd₃N@C₈₀ and hydroxylated Gd₃N@C₈₀ at a dose of $1.67\text{ }\mu\text{mol}$, or a mixture of $25\text{ }\mu\text{mol kg}^{-1}$ free ZD2 and $1.67\text{ }\mu\text{mol}$ ZD2-Gd₃N@C₈₀ (competitive group). Tumor locations are indicated by white arrow heads (d) Analysis of percentage increase of tumor contrast-to-noise ratio (CNR) from images acquired in groups indicated in (c). Reprinted with permission from ref. 122. Copyright 2017 Springer Nature.

Relatedly, a mixture of ZD2-Gd₃N@C₈₀ and free ZD2 demonstrated a loss of contrast enhancement in MDA-MB-231 mice, which is indicative of competitive binding and further support the targeting activity of ZD2-Gd₃N@C₈₀ towards EDB-FN (Fig. 12c,d). MR image analysis of ZD2-Gd₃N@C₈₀ on other representative high- and low-risk breast cancer mice models was performed at a higher field strength of 7 T, and the nano contrast agent still displayed selective and strong signal towards the TNBC mice over a 30-minute analysis period.

Xiao et al. also utilized a Gd₃N@C₈₀ derivative for the differentiation of two conditions; namely, chronic post-traumatic osteomyelitis (CPO) and aseptic inflammation.¹²³ Notably, the early stages of CPO infection share similar pathologies with aseptic inflammation, hampering its early diagnosis. This work investigated the potential utility of IL-13R α 2 as a biomarker for characterizing CPO. The authors designed a carboxylated Gd₃N@C₈₀ derivative attached to a TAMRA-conjugated IL-13 peptide for potential utility as an MRI contrast agent capable of detecting the CPO-related IL-13R α 2 expression. LPS-stimulated and non-stimulated RAW 264.7 cells were treated with the EMF probe, and strong TAMRA fluorescence was observed for the LPS-stimulated cells, which is consistent with its binding to the overexpressed IL-13R α 2 receptor. In vivo MR imaging was also performed on the tibia of CPO mice. Compared to the sham tibia, which was not bacterially infected, the infected tibia exhibited strong contrast enhancement under EMF treatment after 1.5 weeks post-infection. MR images taken after four weeks post-infection displayed multiple inflammatory foci. Thus, the specificity of the EMF probe towards IL-13R α 2 and its high contrast enhancement proved utility in both the initial diagnostic differentiation between CPO and aseptic inflammation as well as the dynamic tracking of CPO-related inflammation.

As mentioned previously, decorating the fullerene surface with positively charged groups can increase its cellular uptake.¹⁰ Thus, implementing a targeting motif and functionalizing the cage with positively-charged ligands facilitates greater cellular binding and uptake, which may facilitate stronger MR contrasts. Li et al. investigated the design of a Gd₃N@C₈₀ derivative ((IL-13-amino)-Ia), which was decorated with hydroxyl and amine moieties and conjugated to a TAMRA-functionalized peptide chain specific towards the overexpressed IL-13R α 2 receptor that is prominent in glioblastoma multiforme (GBM).¹¹⁹ For comparison, a carboxylated version ((IL-13-carboxyl)-IIa) of the EMF derivative was also synthesized, offering insight into the effects of a negatively-charged cage surface. Cell uptake studies were done on U251 GBM cells, and EMF uptake was monitored via fluorescent confocal microscopy. (IL-13-amino)-Ia demonstrated more efficient endocytic uptake compared to (IL-13-carboxyl)-IIa, due to its positively charged amino groups. Furthermore, when incubated into HeLa cells, which lack overexpression of the IL-13R α 2 receptor, neither of the two derivatives displayed significant cell uptake. These results highlight the greater cell uptake offered by a positively-charged nanoparticle and demonstrate the cell specificity of these EMFs towards IL-13R α 2-expressing cells, offered by the targeting peptide. The contrast enhancement of (IL-13-amino)-Ia was then studied in aqueous solution and in vivo. In solution, (IL-13-

amino)-Ia demonstrated very potent contrast as it exhibited similar contrast to Magnevist (a commercial GBCA) of 20-50 times higher concentration. Subsequently, (IL-13-amino)-Ia was injected intravenously via the tail of a U-251 brain tumor mouse model, and consistent with the in vitro study, the more dilute EMF solution displayed a stronger and more localized tumor contrast enhancement compared to Magnevist.

Given the tendency of fullerenes to aggregate in aqueous media,^{124,125} the nanoparticle assembly of metallofullerenes may be leveraged for amplified contrast intensity. By coupling a stimulus to a change in the nanoparticle assembly, an enhanced signal-to-noise ratio may be achieved, similar to that seen in activable fluorescent probes.^{126,127} Particularly, Wang et al. investigated a pH-responsive nano assembly (DOX-RNP) comprised of doxorubicin and a polymer-functionalized Gd₃N@C₈₀.¹²⁸ The polymer contains basic amine groups that are protonated under acidic conditions, causing an increase in the hydrophilicity of the nanoparticle and an accompanying release of the loaded doxorubicin. In addition, the increased hydrophilicity allows for greater interaction between water and the constituent Gd₃N@C₈₀ cages, granting it higher contrast compared to the more hydrophobic DOX-RNPs that exist at physiological pH. Indeed, this study measured a significant increase in both the r_1 values and doxorubicin release from DOX-RNPs when transitioning from physiological pH to a pH of 6.6. The in-vitro results were supported in vivo by measuring the contrast enhancement of tumors in HeLa tumor-bearing mice. DOX-RNPs were injected intravenously into the mice, and MR images at 7 T were assessed at 2, 24, and 48 hours after injection. Tumor-localized contrast was observed early, and at all three time points, there was significant contrast enhancement, indicating an interaction between DOX-RNP and the acidic tumor microenvironment.

A prerequisite of these fullerene-based contrast agents is their water solubility. However, the previously discussed systems were prepared using multiaddition cage functionalizations that generate a variable, heterogeneous mixture of products. Thus, in consideration of the lack of molecularly precise EMF materials, we recently reported a group of structurally well-defined water-soluble EMF derivatives.¹²⁹ The study involved the synthesis of a three-buckyball system, dubbed a “metallobuckytrio” (MBT), consisting of a hexakis-C₆₀ core attached to two M₃N@C₈₀ (M = Lu, Gd) monoadducts via oligoethylene glycol-based (OEG) linkers (Compounds 8b-e, Fig. 13a). Water solubility was then offered by monodisperse PEG attachment to the C₆₀ core through click reactions. Importantly, other biologically relevant ligands, such as targeting moieties, can be clicked onto the MBT platform, highlighting the high modularity of the MBTs for the development of “designer nanoparticles.” These water-soluble MBTs derivatives displayed a tendency to aggregate in water into large structures of sizes ranging from 150-500 nm (Fig. 13b,c). They also exhibited biocompatibility as they showed no metal leakage as monitored by ICP-MS with detection limit below 1 ppb, as well as no cytotoxicity up to 32 μ M towards a range of cell lines, including NIH-3T3 cells, HeLa cells, and induced pluripotent neural stem cells. The T_1 relaxivity of the MBT platform was investigated, and at 1.4 T, it displayed high

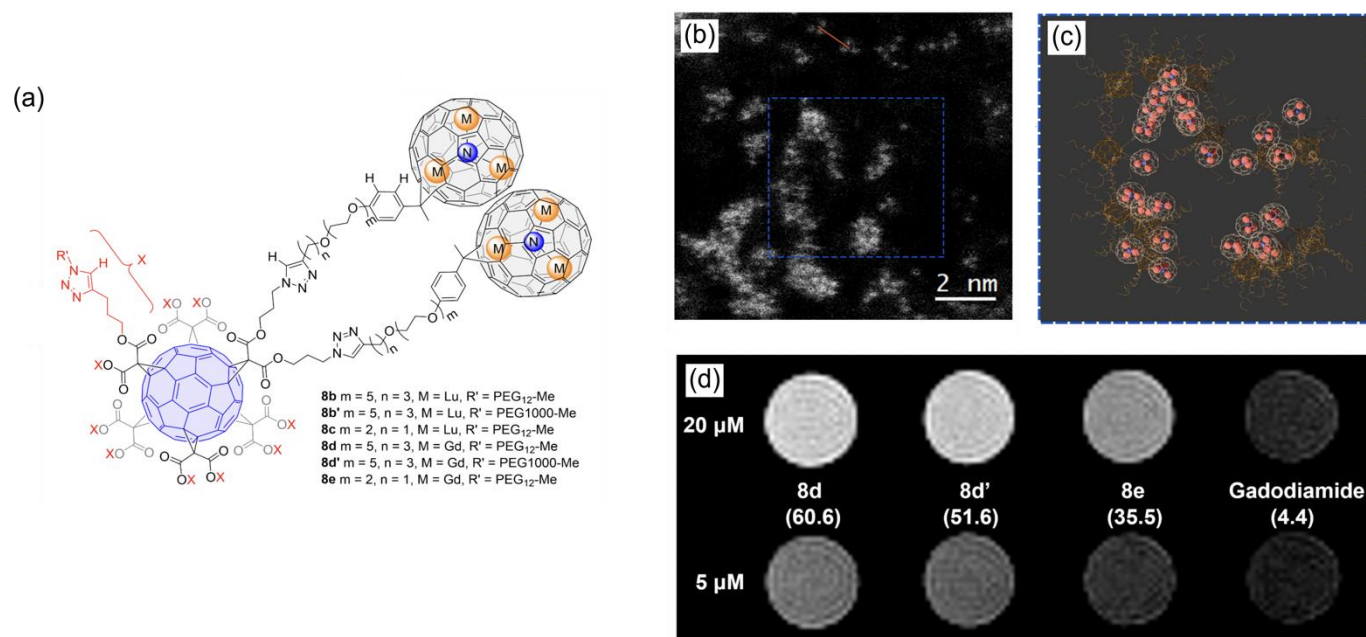


Fig. 13 (a) Structure of MBT platform with PEG ligands. (b) High-angle annular dark-field (HAADF) STEM image of 8e. (c) Schematic representation of the area in the blue dotted line in (b), exemplifying the possible positions of the C₆₀ core and ligands that are barely visible in the HAADF image. (d) MR imaging of Gd MBT solutions on a 1.0 T scanner. The measured r₁ values at 1.4 T are written in parentheses under each compound, in the unit of mM⁻¹s⁻¹. Reprinted with permission from ref. 129. Copyright 2022 John Wiley and Sons.

r₁ values between 30–60 mM⁻¹s⁻¹. Indeed, MR imaging of various MBT solutions highlighted the significantly higher contrast enhancement observed with the MBT platform compared to gadodiamide (Fig. 13d). The higher contrast enhancement was mainly ascribed the higher aggregation size, and increased water attraction from the OEG linkers. However, due to the lack of exchangeable protons near the Gd ions, the relaxivity of the MBT derivatives are considerably lower than the high-relaxivity EMF GBAs, leaving a critical future research direction open to explore. In addition to the promising diagnostic potential, its therapeutic character was also assessed. As monitored by EPR, irradiation of various MBT derivatives with a green LED prompted the generation of both type I and type II ROS, with a preference of the Type I mechanism. Previous reports have investigated fullerene systems capable of pleiotropic effects spanning multiple modes of imaging and therapeutic effect;^{130–132} however, the MBT platform represents an opportunity for molecularly precise nanoparticles of high modularity.

7. Conclusion

This review explored the utility of fullerene compounds for biomedical materials and discussed potential avenues for the applications and design of these systems. The molecular structure of fullerene and its derivatives allows for tailorable structure and function, making them ideal candidates for precision medicine. Their applications span multiple areas, each potentially benefitting from the diverse organelle accumulation of these materials, ranging from the cell membrane, lysosomes, nucleus, and mitochondria. We have discussed fullerenes in their utility in drug delivery, where they can act as monodisperse drug carriers for a variety of ligands spanning small molecules to large

biomolecules such as nucleic acids. Many fullerene systems are also anti-inflammatory and antioxidant, which can be carefully tuned to achieve a pleiotropic therapeutic effect on the organismal level. Upon irradiation with light, these systems can display a juxtaposing pro-oxidative function, spawning the generation of ROS that can be utilized in PDT. Finally, the encapsulation of gadolinium and gadolinium-based clusters within fullerene cages allows a robust containment of this toxic yet appealing MRI contrast agent. Ultimately, fullerene materials pose great advantages for the areas of medicine, biotechnology, and fundamental biological study, and the increasing attention towards tailorable and precise medicine may find promise in the rational design of these systems.

Conflicts of interest

There are no conflicts to declare.

Acknowledgements

A.D. would like to acknowledge the support from the Jerome and Lorraine Aresty Undergraduate Research Scholarship from School of Arts and Sciences, Rutgers University. We thank the Busch Biomedical Grant and the US Department of Energy (DE-SC0020260) for support of this work.

References

- 1 M. J. Mitchell, M. M. Billingsley, R. M. Haley, M. E. Wechsler, N. A. Peppas and R. Langer, Engineering precision nanoparticles for drug delivery, *Nat. Rev. Drug Discov.*, 2021, **20**, 101–124.

- 2 C. T. Jafvert and P. P. Kulkarni, Buckminsterfullerene's (C_{60}) octanol-water partition coefficient (K_{ow}) and aqueous solubility, *Environ. Sci. Technol.*, 2008, **42**, 5945–5950.
- 3 A. Törpe and D. J. Belton, Improved spectrophotometric analysis of fullerenes C_{60} and C_{70} in high-solubility organic solvents, *Anal. Sci.*, 2015, **31**, 125–130.
- 4 P. P. Fatouros, F. D. Corwin, Z.-J. Chen, W. C. Broaddus, J. L. Tatum, B. Kettenmann, Z. Ge, H. W. Gibson, J. L. Russ and A. P. Leonard, In vitro and in vivo imaging studies of a new endohedral metallofullerene nanoparticle, *Radiology*, 2006, **240**, 756–764.
- 5 M. D. Shultz, J. D. Wilson, C. E. Fuller, J. Zhang, H. C. Dorn and P. P. Fatouros, Metallofullerene-based nanoplatform for brain tumor brachytherapy and longitudinal imaging in a murine orthotopic xenograft model, *Radiology*, 2011, **261**, 136–143.
- 6 R. Biswas, S. Yang, R. A. Crichton, P. Adly-Gendi, T. K. Chen, W. P. Kopcha, Z. Shi and J. Zhang, C_{60} - β -cyclodextrin conjugates for enhanced nucleus delivery of doxorubicin, *Nanoscale*, 2022, **14**, 4456–4462.
- 7 H. Isobe, W. Nakanishi, N. Tomita, S. Jinno, H. Okayama and E. Nakamura, Nonviral gene delivery by tetraamino fullerene, *Mol. Pharmaceutics*, 2006, **3**, 124–134.
- 8 A. Muñoz, D. Sigwalt, B. M. Illescas, J. Luczkowiak, L. Rodríguez-Pérez, I. Nierengarten, M. Holler, J.-S. Remy, K. Buffet, S. P. Vincent, J. Rojo, R. Delgado, J.-F. Nierengarten and N. Martín, Synthesis of giant globular multivalent glycofullerenes as potent inhibitors in a model of Ebola virus infection, *Nat. Chem.*, 2016, **8**, 50–57.
- 9 J. Zhang, J. Xu, H. Ma, H. Bai, L. Liu, C. Shu, H. Li, S. Wang and C. Wang, Designing an amino-fullerene derivative C_{70} -(EDA)₈ to fight super bacteria, *ACS Appl. Mater. Interfaces*, 2019, **11**, 14597–14607.
- 10 H. Ma, X. Zhang, Y. Yang, S. Li, J. Huo, Y. Liu, M. Guan, M. Zhen, C. Shu, J. Li and C. Wang, Cellular uptake, organelle enrichment, and in vitro antioxidation of fullerene derivatives, mediated by surface charge, *Langmuir*, 2021, **37**, 2740–2748.
- 11 H. Ma, J. Zhao, H. Meng, D. Hu, Y. Zhou, X. Zhang, C. Wang, J. Li, J. Yuan and Y. Wei, Carnosine-modified fullerene as a highly enhanced ROS scavenger for mitigating acute oxidative stress, *ACS Appl. Mater. Interfaces*, 2020, **12**, 16104–16113.
- 12 L. Xiao, R. Huang, N. Sulimai, R. Yao, B. Manley, P. Xu, R. Felder, L. Jin, H. C. Dorn and X. Li, Amine functionalized trimetallic nitride endohedral fullerenes: a class of nanoparticle to tackle low back/leg pain, *ACS Appl. Bio Mater.*, 2022, **5**, 2943–2955.
- 13 H. Shi, R. Gu, W. Xu, H. Huang, L. Xue, W. Wang, Y. Zhang, W. Si and X. Dong, Near-infrared light-harvesting fullerene-based nanoparticles for promoted synergetic tumor phototheranostics, *ACS Appl. Mater. Interfaces*, 2019, **11**, 44970–44977.
- 14 Q. Tang, W. Xiao, J. Li, D. Chen, Y. Zhang, J. Shao and X. Dong, A fullerene-rhodamine B photosensitizer with pH-activated visible-light absorbance/fluorescence/photodynamic therapy, *J. Mater. Chem. B*, 2018, **6**, 2778–2784.
- 15 M. Serda, M. J. Ware, J. M. Newton, S. Sachdeva, M. Krzykawska-Serda, L. Nguyen, J. Law, A. O. Anderson, S. A. Curley, L. J. Wilson and S. J. Corr, Development of photoactive sweet- C_{60} for pancreatic cancer stellate cell therapy, *Nanomedicine*, 2018, **13**, 2981–2993.
- 16 C.-W. Wong, A. V. Zhilenkov, O. A. Kraevaya, D. V. Mischenko, P. A. Troshin and S. Hsu, Toward understanding the antitumor effects of water-soluble fullerene derivatives on lung cancer cells: Apoptosis or autophagy pathways?, *J. Med. Chem.*, 2019, **62**, 7111–7125.
- 17 J. Huo, J. Li, Y. Liu, L. Yang, X. Cao, C. Zhao, Y. Lu, W. Zhou, S. Li, J. Liu, J. Li, X. Li, J. Wan, R. Wen, M. Zhen, C. Wang and C. Bai, Amphiphilic aminated derivatives of [60]fullerene as potent inhibitors of tumor growth and metastasis, *Adv. Sci.*, 2022, **9**, 2201541.
- 18 A. I. Archakov, V. M. Govorun, A. V. Dubanov, Y. D. Ivanov, A. V. Veselovsky, P. Lewi and P. Janssen, Protein-protein interactions as a target for drugs in proteomics, *Proteomics*, 2003, **3**, 380–391.
- 19 E. Castro, A. H. Garcia, G. Zavala and L. Echegoyen, Fullerenes in biology and medicine, *J. Mater. Chem. B*, 2017, **5**, 6523–6535.
- 20 I. Rašović, Water-soluble fullerenes for medical applications, *Mater. Sci. Technol.*, 2017, **33**, 777–794.
- 21 M. Yamada, S. Nagase and T. Akasaka, in *Handbook of Fullerene Science and Technology*, eds. X. Lu, T. Akasaka and Z. Slanina, Springer Singapore, Singapore, 2021, pp. 1–50.
- 22 I. Donskyi, M. Drüke, K. Silberreis, D. Lauster, K. Ludwig, C. Kühne, W. Unger, C. Böttcher, A. Herrmann, J. Dornedde, M. Adeli and R. Haag, Interactions of fullerene-polyglycerol sulfates at viral and cellular interfaces, *Small*, 2018, **14**, 1800189.
- 23 Y. Sun, A. Kakinen, C. Zhang, Y. Yang, A. Faridi, T. P. Davis, W. Cao, P. C. Ke and F. Ding, Amphiphilic surface chemistry of fullerenols is necessary for inhibiting the amyloid aggregation of alpha-synuclein NACore, *Nanoscale*, 2019, **11**, 11933–11945.
- 24 M. Chen, S. Zhou, L. Guo, L. Wang, F. Yao, Y. Hu, H. Li and J. Hao, Aggregation behavior and antioxidant properties of amphiphilic fullerene C_{60} derivatives cofunctionalized with cationic and nonionic hydrophilic groups, *Langmuir*, 2019, **35**, 6939–6949.
- 25 E. Okutan, in *Fullerenes and Relative Materials Properties and Application*, ed. N. Kamanina, IntechOpen, United Kingdom, 2018, 127–143.
- 26 J. Zhao, W. Wu, J. Sun and S. Guo, Triplet photosensitizers: from molecular design to applications, *Chem. Soc. Rev.*, 2013, **42**, 5323–5351.
- 27 Q. Kong, J. A. Beel and K. O. Lillehei, A threshold concept for cancer therapy, *Med. Hypotheses*, 2000, **55**, 29–35.
- 28 L. Jin, M. Ding, A. Oklopčić, B. Aghdasi, L. Xiao, Z. Li, V. Jevtovic-Todorovic and X. Li, Nanoparticle fullerol alleviates radiculopathy via NLRP3 inflammasome and neuropeptides, *Nanomedicine*, 2017, **13**, 2049–2059.
- 29 S. Liu, D. Chen, X. Li, M. Guan, Y. Zhou, L. Li, W. Jia, C. Zhou, C. Shu, C. Wang and C. Bai, Fullerene nanoparticles: a promising candidate for the alleviation of silicosis-associated pulmonary inflammation, *Nanoscale*, 2020, **12**, 17470–17479.
- 30 W. Shen, L. Bao and X. Lu, Endohedral metallofullerenes: an ideal platform of sub-nano chemistry, *Chin. J. Chem.*, 2022, **40**, 275–284.
- 31 T. Wang and C. Wang, Functional metallofullerene materials and their applications in nanomedicine, magnetism, and electronics, *Small*, 2019, **15**, 1901522.
- 32 T. Li and H. C. Dorn, Biomedical applications of metal-encapsulated fullerene nanoparticles, *Small*, 2017, **13**, 1603152.
- 33 R. Wang, X. Li and J. Yoon, Organelle-targeted photosensitizers for precision photodynamic therapy, *ACS Appl. Mater. Interfaces*, 2021, **13**, 19543–19571.
- 34 W.-C. Hou, B. Y. Moghadam, P. Westerhoff and J. D. Posner, Distribution of fullerene nanomaterials between water and model biological membranes, *Langmuir*, 2011, **27**, 11899–11905.
- 35 J. Wong-Ekkabut, S. Baoukina, W. Triampo, I.-M. Tang, D. P. Tieleman and L. Monticelli, Computer simulation study of

- fullerene translocation through lipid membranes, *Nat. Nanotechnol.*, 2008, **3**, 363–368.
- 36 O. K. Nag, M. H. Stewart, J. R. Deschamps, K. Susumu, E. Oh, V. Tsytsarev, Q. Tang, A. L. Efros, R. Vaxenburg, B. J. Black, Y. Chen, T. J. O'Shaughnessy, S. H. North, L. D. Field, P. E. Dawson, J. J. Pancrazio, I. L. Medintz, Y. Chen, R. S. Erzurumlu, A. L. Huston and J. B. Delehanty, Quantum dot–peptide–fullerene bioconjugates for visualization of in vitro and in vivo cellular membrane potential, *ACS Nano*, 2017, **11**, 5598–5613.
- 37 T.-Y. Wang, M. D. J. Libardo, A. M. Angeles-Boza and J.-P. Pellois, Membrane oxidation in cell delivery and cell killing applications, *ACS Chem. Biol.*, 2017, **12**, 1170–1182.
- 38 R. Shimada, S. Hino, K. Yamana, R. Kawasaki, T. Konishi and A. Ikeda, Improvement of photodynamic activity by a stable system consisting of a C₆₀ derivative and photoantenna in liposomes, *ACS Med. Chem. Lett.*, 2022, **13**, 641–647.
- 39 S. Kraszewski, M. Tarek and C. Ramseyer, Uptake and translocation mechanisms of cationic amino derivatives functionalized on pristine C₆₀ by lipid membranes: a molecular dynamics simulation study, *ACS Nano*, 2011, **5**, 8571–8578.
- 40 I. Canton and G. Battaglia, Endocytosis at the nanoscale, *Chem. Soc. Rev.*, 2012, **41**, 2718–2739.
- 41 W. Li, C. Chen, C. Ye, T. Wei, Y. Zhao, F. Lao, Z. Chen, H. Meng, Y. Gao, H. Yuan, G. Xing, F. Zhao, Z. Chai, X. Zhang, F. Yang, D. Han, X. Tang and Y. Zhang, The translocation of fullerene nanoparticles into lysosome via the pathway of clathrin-mediated endocytosis, *Nanotechnology*, 2008, **19**, 145102.
- 42 L. W. Zhang, J. Yang, A. R. Barron and N. A. Monteiro-Riviere, Endocytic mechanisms and toxicity of a functionalized fullerene in human cells, *Toxicol. Lett.*, 2009, **191**, 149–157.
- 43 M. Lucafò, S. Pacor, C. Fabbro, T. Da Ros, S. Zorzet, M. Prato and G. Sava, Study of a potential drug delivery system based on carbon nanoparticles: effects of fullerene derivatives in MCF7 mammary carcinoma cells, *J. Nanopart. Res.*, 2012, **14**, 830.
- 44 S. A. Smith, L. I. Selby, A. P. R. Johnston and G. K. Such, The endosomal escape of nanoparticles: toward more efficient cellular delivery, *Bioconjugate Chem.*, 2019, **30**, 263–272.
- 45 Y.-B. Hu, E. B. Dammer, R.-J. Ren and G. Wang, The endosomal-lysosomal system: from acidification and cargo sorting to neurodegeneration, *Transl. Neurodegener.*, 2015, **4**, 18.
- 46 J. A. Mindell, Lysosomal acidification mechanisms, *Annu. Rev. Physiol.*, 2012, **74**, 69–86.
- 47 M. Gangopadhyay, S. K. Mukhopadhyay, S. Gayathri, S. Biswas, S. Barman, S. Dey and N. D. P. Singh, Fluorene–morpholine-based organic nanoparticles: lysosome-targeted pH-triggered two-photon photodynamic therapy with fluorescence switch on–off, *J. Mater. Chem. B*, 2016, **4**, 1862–1868.
- 48 B. Lozano-Torres, J. F. Blandez, I. Galiana, J. A. Lopez-Dominguez, M. Rovira, M. Paez-Ribes, E. González-Gualda, D. Muñoz-Espín, M. Serrano, F. Sancenón and R. Martínez-Mañez, A two-photon probe based on naphthalimide-styrene fluorophore for the in vivo tracking of cellular senescence, *Anal. Chem.*, 2021, **93**, 3052–3060.
- 49 X. Li, Y. Pan, H. Chen, Y. Duan, S. Zhou, W. Wu, S. Wang and B. Liu, specific near-infrared probe for ultrafast imaging of lysosomal β -galactosidase in ovarian cancer cells, *Anal. Chem.*, 2020, **92**, 5772–5779.
- 50 I. S. Donskyi, K. Achazi, V. Wycisk, K. Licha, M. Adeli and R. Haag, Fullerene polyglycerol amphiphiles as unimolecular transporters, *Langmuir*, 2017, **33**, 6595–6600.
- 51 P. Chaudhuri, A. Paraskar, S. Soni, R. A. Mashelkar and S. Sengupta, Fullerenol–cytotoxic conjugates for cancer chemotherapy, *ACS Nano*, 2009, **3**, 2505–2514.
- 52 M. Di Giosia, A. Soldà, M. Seeger, A. Cantelli, F. Arnesano, M. I. Nardella, V. Mangini, F. Valle, M. Montalti, F. Zerbetto, S. Rapino, M. Calvaresi and V. Ntziachristos, A bioconjugated fullerene as a subcellular-targeted and multifaceted phototheranostic agent, *Adv. Funct. Mater.*, 2021, **31**, 2101527.
- 53 B.-B. S. Zhou and S. J. Elledge, The DNA damage response: putting checkpoints in perspective, *Nature*, 2000, **408**, 433–439.
- 54 D. S. Kwag, K. Park, K. T. Oh and E. S. Lee, Hyaluronated fullerenes with photoluminescent and antitumoral activity, *Chem. Commun.*, 2013, **49**, 282–284.
- 55 J. Fan, G. Fang, F. Zeng, X. Wang and S. Wu, Water-dispersible fullerene aggregates as a targeted anticancer prodrug with both chemo- and photodynamic therapeutic actions, *Small*, 2013, **9**, 613–621.
- 56 S. Foley, C. Crowley, M. Smaih, C. Bonfils, B. F. Erlanger, P. Seta and C. Larroque, Cellular localisation of a water-soluble fullerene derivative, *Biochem. Biophys. Res. Commun.*, 2002, **294**, 116–119.
- 57 S. S. Ali, J. I. Hardt, K. L. Quick, J. Sook Kim-Han, B. F. Erlanger, T. Huang, C. J. Epstein and L. L. Dugan, A biologically effective fullerene (C₆₀) derivative with superoxide dismutase mimetic properties, *Free Radical Biol. Med.*, 2004, **37**, 1191–1202.
- 58 M. N. Martinez and G. L. Amidon, A mechanistic approach to understanding the factors affecting drug absorption: a review of fundamentals, *J. Clin. Pharmacol.*, 2002, **42**, 620–643.
- 59 A. Agostini, L. Mondragón, A. Bernardos, R. Martínez-Mañez, M. D. Marcos, F. Sancenón, J. Soto, A. Costero, C. Manguan-García, R. Perona, M. Moreno-Torres, R. Aparicio-Sanchis and J. R. Murguía, Targeted cargo delivery in senescent cells using capped mesoporous silica nanoparticles, *Angew. Chem., Int. Ed.*, 2012, **51**, 10556–10560.
- 60 T. Yong, X. Zhang, N. Bie, H. Zhang, X. Zhang, F. Li, A. Hakeem, J. Hu, L. Gan, H. A. Santos and X. Yang, Tumor exosome-based nanoparticles are efficient drug carriers for chemotherapy, *Nat. Commun.*, 2019, **10**, 3838.
- 61 M. Raoof, Y. Mackeyev, M. A. Cheney, L. J. Wilson and S. A. Curley, Internalization of C₆₀ fullerenes into cancer cells with accumulation in the nucleus via the nuclear pore complex, *Biomaterials*, 2012, **33**, 2952–2960.
- 62 N. A. Lapin, L. A. Vergara, Y. Mackeyev, J. M. Newton, S. A. Dilliard, L. J. Wilson, S. A. Curley and R. E. Serda, Biotransport kinetics and intratumoral biodistribution of malonodiserialamide-derivatized [60] fullerene in a murine model of breast adenocarcinoma, *Int. J. Nanomed.*, 2017, **12**, 8289–8307.
- 63 T. Y. Zakharian, A. Seryshev, B. Sitharaman, B. E. Gilbert, V. Knight and L. J. Wilson, A fullerene–paclitaxel chemotherapeutic: synthesis, characterization, and study of biological activity in tissue culture, *J. Am. Chem. Soc.*, 2005, **127**, 12508–12509.
- 64 M. Kumar, G. Sharma, R. Kumar, B. Singh, O. P. Katore and K. Raza, Lysine-based C₆₀-fullerene nanoconjugates for monomethyl fumarate delivery: a novel nanomedicine for brain cancer cells, *ACS Biomater. Sci. Eng.*, 2018, **4**, 2134–2142.
- 65 X. Liu, Y. Chen, H. Li, N. Huang, Q. Jin, K. Ren and J. Ji, Enhanced retention and cellular uptake of nanoparticles in tumors by controlling their aggregation behavior, *ACS Nano*, 2013, **7**, 6244–6257.
- 66 L. Wang, J. Huang, H. Chen, H. Wu, Y. Xu, Y. Li, H. Yi, Y. A. Wang, L. Yang and H. Mao, Exerting enhanced

- permeability and retention effect driven delivery by ultrafine iron oxide nanoparticles with T_1 – T_2 switchable magnetic resonance imaging contrast, *ACS Nano*, 2017, **11**, 4582–4592.
- 67 B. Genabeek, B. A. G. Lamers, C. J. Hawker, E. W. Meijer, W. R. Gutekunst and B. V. K. J. Schmidt, Properties and applications of precision oligomer materials; where organic and polymer chemistry join forces, *J. Polym. Sci.*, 2021, **59**, 373–403.
- 68 H. Li, B. Zhang, X. Lu, X. Tan, F. Jia, Y. Xiao, Z. Cheng, Y. Li, D. O. Silva, H. S. Schrekker, K. Zhang and C. A. Mirkin, Molecular spherical nucleic acids, *Proc. Natl. Acad. Sci. U.S.A.*, 2018, **115**, 4340–4344.
- 69 H. Li, Y. Li, Y. Xiao, B. Zhang, Z. Cheng, J. Shi, J. Xiong, Z. Li and K. Zhang, Well-defined DNA–polymer miktoarm stars for enzyme-resistant nanoflakes and carrier-free gene regulation, *Bioconjugate Chem.*, 2020, **31**, 530–536.
- 70 P. L. Felgner, T. R. Gadek, M. Holm, R. Roman, H. W. Chan, M. Wenz, J. P. Northrop, G. M. Ringold and M. Danielsen, Lipofection: a highly efficient, lipid-mediated DNA-transfection procedure, *Proc. Natl. Acad. Sci. U.S.A.*, 1987, **84**, 7413–7417.
- 71 J.-P. Yang and L. Huang, Overcoming the inhibitory effect of serum on lipofection by increasing the charge ratio of cationic liposome to DNA, *Gene Therapy*, 1997, **4**, 950–960.
- 72 Z. Dong, L. Feng, Y. Chao, Y. Hao, M. Chen, F. Gong, X. Han, R. Zhang, L. Cheng and Z. Liu, Amplification of tumor oxidative stresses with liposomal Fenton catalyst and glutathione inhibitor for enhanced cancer chemotherapy and radiotherapy, *Nano Lett.*, 2019, **19**, 805–815.
- 73 D. Shi, G. Mi, Y. Shen and T. J. Webster, Glioma-targeted dual functionalized thermosensitive Ferri-liposomes for drug delivery through an in vitro blood–brain barrier, *Nanoscale*, 2019, **11**, 15057–15071.
- 74 H. Y. Yoon, H. M. Yang, C. H. Kim, Y. T. Goo, G. Y. Hwang, I. H. Chang, Y. M. Whang and Y. W. Choi, Enhanced intracellular delivery of BCG cell wall skeleton into bladder cancer cells using liposomes functionalized with folic acid and Pep-1 peptide, *Pharmaceutics*, 2019, **11**, 652.
- 75 R. Partha, L. R. Mitchell, J. L. Lyon, P. P. Joshi and J. L. Conyers, Buckysomes: fullerene-based nanocarriers for hydrophobic molecule delivery, *ACS Nano*, 2008, **2**, 1950–1958.
- 76 R. Partha, M. Lackey, A. Hirsch, S. W. Casscells and J. L. Conyers, Self assembly of amphiphilic C_{60} fullerene derivatives into nanoscale supramolecular structures, *J. Nanobiotechnol.*, 2007, **5**, 6.
- 77 K. Minami, K. Okamoto, K. Harano, E. Noiri and E. Nakamura, Hierarchical assembly of siRNA with tetraamino fullerene in physiological conditions for efficient internalization into cells and knockdown, *ACS Appl. Mater. Interfaces*, 2018, **10**, 19347–19354.
- 78 K. Minami, K. Okamoto, K. Doi, K. Harano, E. Noiri and E. Nakamura, siRNA delivery targeting to the lung via agglutination-induced accumulation and clearance of cationic tetraamino fullerene, *Sci. Rep.*, 2014, **4**, 4916.
- 79 D. Trachootham, J. Alexandre and P. Huang, Targeting cancer cells by ROS-mediated mechanisms: a radical therapeutic approach?, *Nat. Rev. Drug Discov.*, 2009, **8**, 579–591.
- 80 S. Suzuki, N. Fujita, N. Hosogane, K. Watanabe, K. Ishii, Y. Toyama, K. Takubo, K. Horiuchi, T. Miyamoto, M. Nakamura and M. Matsumoto, Excessive reactive oxygen species are therapeutic targets for intervertebral disc degeneration, *Arthritis Res. Ther.*, 2015, **17**, 316.
- 81 H. Ueno, S. Yamakura, R. S. Arastoo, T. Oshima and K. Kokubo, Systematic evaluation and mechanistic investigation of antioxidant activity of fullerenols using β -carotene bleaching assay, *J. Nanomater.*, 2014, **2014**, 802596.
- 82 J. Grebowski, A. Krokosz, A. Konarska, M. Wolszczak and M. Puchala, Rate constants of highly hydroxylated fullerene C_{60} interacting with hydroxyl radicals and hydrated electrons. Pulse radiolysis study, *Radiat. Phys. Chem.*, 2014, **103**, 146–152.
- 83 S. H. Friedman, D. L. DeCamp, R. P. Sijbesma, G. Srdanov, F. Wudl and G. L. Kenyon, Inhibition of the HIV-1 protease by fullerene derivatives: model building studies and experimental verification, *J. Am. Chem. Soc.*, 1993, **115**, 6506–6509.
- 84 Y. Pan, L. Wang, S. Kang, Y. Lu, Z. Yang, T. Huynh, C. Chen, R. Zhou, M. Guo and Y. Zhao, Gd–metallofullerenol nanomaterial suppresses pancreatic cancer metastasis by inhibiting the interaction of histone deacetylase 1 and metastasis-associated protein 1, *ACS Nano*, 2015, **9**, 6826–6836.
- 85 P. Roy, S. Bag, D. Chakraborty and S. Dasgupta, Exploring the inhibitory and antioxidant effects of fullerene and fullerene on ribonuclease A, *ACS Omega*, 2018, **3**, 12270–12283.
- 86 D. Balasubramanian and R. Kanwar, in *Oxygen/Nitrogen Radicals: Cell Injury and Disease*, eds. V. Vallyathan, X. Shi and V. Castranova, Springer US, Boston, MA, 2002, pp. 27–38.
- 87 M. Calvaresi, F. Arnesano, S. Bonacchi, A. Bottoni, V. Calò, S. Conte, G. Falini, S. Fermani, M. Losacco, M. Montalti, G. Natile, L. Prodi, F. Sparla and F. Zerbetto, C_{60} @Lysozyme: direct observation by nuclear magnetic resonance of a 1:1 fullerene protein adduct, *ACS Nano*, 2014, **8**, 1871–1877.
- 88 L. L. Dugan, D. M. Turetsky, C. Du, D. Lobner, M. Wheeler, C. R. Almlı, C. K.-F. Shen, T.-Y. Luh, D. W. Choi and T.-S. Lin, Carboxyfullerenes as neuroprotective agents, *Proc. Natl. Acad. Sci. U.S.A.*, 1997, **94**, 9434–9439.
- 89 L. Xiao, R. Huang, Y. Zhang, T. Li, J. Dai, N. Nannapuneni, T. R. Chastanet, M. Chen, F. H. Shen, L. Jin, H. C. Dorn and X. Li, A new formyl peptide receptor-1 antagonist conjugated fullerene nanoparticle for targeted treatment of degenerative disc diseases, *ACS Appl. Mater. Interfaces*, 2019, **11**, 38405–38416.
- 90 J. Li, M. Guan, T. Wang, M. Zhen, F. Zhao, C. Shu and C. Wang, Gd@C₈₂-(ethylenediamine)₈ nanoparticle: a new high-efficiency water-soluble ROS scavenger, *ACS Appl. Mater. Interfaces*, 2016, **8**, 25770–25776.
- 91 O. V. Boltalina, I. N. Ioffe, I. D. Sorokin and L. N. Sidorov, Electron affinity of some endohedral lanthanide fullerenes, *J. Phys. Chem. A*, 1997, **101**, 9561–9563.
- 92 C. Zhou, M. Zhen, M. Yu, X. Li, T. Yu, J. Liu, W. Jia, S. Liu, L. Li, J. Li, Z. Sun, Z. Zhao, X. Wang, X. Zhang, C. Wang and C. Bai, Gadofullerene inhibits the degradation of apolipoprotein B100 and boosts triglyceride transport for reversing hepatic steatosis, *Sci. Adv.*, 2020, **6**, eabc1586.
- 93 F. Nassir, R. S. Rector, G. M. Hammoud and J. A. Ibdah, Pathogenesis and prevention of hepatic steatosis, *Gastroenterol. Hepatol.*, 2015, **11**, 167–175.
- 94 S. Hekimi, J. Lapointe and Y. Wen, Taking a “good” look at free radicals in the aging process, *Trends Cell Biol.*, 2011, **21**, 569–576.
- 95 Y. Zhou, M. Zhen, H. Ma, J. Li, C. Shu and C. Wang, Inhalable gadofullerenol/[70] fullerene as high-efficiency ROS scavengers for pulmonary fibrosis therapy, *Nanomedicine*, 2018, **14**, 1361–1369.
- 96 J.-F. Pittet, M. J. D. Griffiths, T. Geiser, N. Kaminski, S. L. Dalton, X. Huang, L. A. S. Brown, P. J. Gotwals, V. E. Kotliansky, M. A. Matthay and D. Sheppard, TGF- β is a critical mediator of acute lung injury, *J Clin Invest*, 2001, **107**, 1537–1544.
- 97 K. Kokubo, K. Matsubayashi, H. Tategaki, H. Takada and T. Oshima, Facile synthesis of highly water-soluble fullerenes

- more than half-covered by hydroxyl groups, *ACS Nano*, 2008, **2**, 327–333.
- 98 W. Cong, P. Wang, Y. Qu, J. Tang, R. Bai, Y. Zhao, Chunying Chen and X. Bi, Evaluation of the influence of fullereneol on aging and stress resistance using *Caenorhabditis elegans*, *Biomaterials*, 2015, **42**, 78–86.
- 99 R. Injac, M. Perse, M. Cerne, N. Potocnik, N. Radic, B. Govedarica, A. Djordjevic, A. Cerar and B. Strukelj, Protective effects of fullereneol C₆₀(OH)₂₄ against doxorubicin-induced cardiotoxicity and hepatotoxicity in rats with colorectal cancer, *Biomaterials*, 2009, **30**, 1184–1196.
- 100 X. Yang, Y. Wan, X. Qiao, V. Arlet and X. Li, Transcriptional alteration of matrix-related gene expression in cultured human disc cells by nanoparticles of a bismethanophosphonate fullerene, *Cell Biol. Int.*, 2010, **34**, 837–844.
- 101 M. R. Hamblin, Fullerenes as photosensitizers in photodynamic therapy: pros and cons, *Photochem. Photobiol. Sci.*, 2018, **17**, 1515–1533.
- 102 D. E. J. G. J. Dolmans, D. Fukumura and R. K. Jain, Photodynamic therapy for cancer, *Nat. Rev. Cancer*, 2003, **3**, 380–387.
- 103 K. Liosi, A. J. Stasyuk, F. Masero, A. A. Voityuk, T. Nauser, V. Mougel, M. Solá and Y. Yamakoshi, Unexpected disparity in photoinduced reactions of C₆₀ and C₇₀ in water with the generation of O₂^{•-} or ¹O₂, *JACS Au*, 2021, **1**, 1601–1611.
- 104 Q. Liu, M. Guan, L. Xu, C. Shu, C. Jin, J. Zheng, X. Fang, Y. Yang and C. Wang, Structural effect and mechanism of C₇₀-carboxyfullerenes as efficient sensitizers against cancer cells, *Small*, 2012, **8**, 2070–2077.
- 105 E. Ö. Gündüz, M. E. Gedik, G. Günaydın and E. Okutan, Amphiphilic fullerene-BODIPY photosensitizers for targeted photodynamic therapy, *ChemMedChem*, 2022, **17**, e202100693.
- 106 H. Ünlü and E. Okutan, Preparation of BODIPY- fullerene and monostyryl BODIPY-fullerene dyads as heavy atom free singlet oxygen generators, *Dyes Pigm.*, 2017, **142**, 340–349.
- 107 R. Ziesse, B. D. Allen, D. B. Rewinska and A. Harriman, Selective triplet-state formation during charge recombination in a fullerene/bodipy molecular dyad (bodipy=borondipyromethene), *Chem. – Eur. J.*, 2009, **15**, 7382–7393.
- 108 L. Huang, X. Yu, W. Wu and J. Zhao, Styryl bodipy-C₆₀ dyads as efficient heavy-atom-free organic triplet photosensitizers, *Org. Lett.*, 2012, **14**, 2594–2597.
- 109 Y. Li, T. Lin, Y. Luo, Q. Liu, W. Xiao, W. Guo, D. Lac, H. Zhang, C. Feng, S. Wachsmann-Hogiu, J. H. Walton, S. R. Cherry, D. J. Rowland, D. Kukis, C. Pan and K. S. Lam, A smart and versatile theranostic nanomedicine platform based on nanoporphyrin, *Nat. Commun.*, 2014, **5**, 4712.
- 110 H. Cheng, G.-L. Fan, J.-H. Fan, L.-P. Zhao, R.-R. Zheng, X.-Y. Yu and S.-Y. Li, Ratiometric theranostic nanoprobe for pH imaging-guided photodynamic therapy, *Nanoscale*, 2019, **11**, 9008–9014.
- 111 C. S. Foote, in *Electron Transfer I*, ed. J. Mattay, Springer Berlin Heidelberg, Berlin, Heidelberg, 1994, pp. 347–363.
- 112 B. P. Toole, Hyaluronan: from extracellular glue to pericellular cue, *Nat. Rev. Cancer*, 2004, **4**, 528–539.
- 113 R. J. McDonald, J. S. McDonald, D. F. Kallmes, M. E. Jentoft, D. L. Murray, K. R. Thielen, E. E. Williamson and L. J. Eckel, Intracranial gadolinium deposition after contrast-enhanced MR imaging, *Radiology*, 2015, **275**, 772–782.
- 114 T. Kanda, T. Fukusato, M. Matsuda, K. Toyoda, H. Oba, J. Kotoku, T. Haruyama, K. Kitajima and S. Furui, Gadolinium-based contrast agent accumulates in the brain even in subjects without severe renal dysfunction: evaluation of autopsy brain specimens with inductively coupled plasma mass spectrometry, *Radiology*, 2015, **276**, 228–232.
- 115 P. Marckmann, L. Skov, K. Rossen, A. Dupont, M. B. Damholt, J. G. Heaf and H. S. Thomsen, Nephrogenic systemic fibrosis: suspected causative role of gadodiamide used for contrast-enhanced magnetic resonance imaging, *J. Am. Soc. Nephrol.*, 2006, **17**, 2359.
- 116 H. Li and T. J. Meade, Molecular magnetic resonance imaging with Gd(III)-based contrast agents: challenges and key advances, *J. Am. Chem. Soc.*, 2019, **141**, 17025–17041.
- 117 J. Zhang, Y. Ye, Y. Chen, C. Pregot, T. Li, S. Balasubramaniam, D. B. Hobart, Y. Zhang, S. Wi, R. M. Davis, L. A. Madsen, J. R. Morris, S. M. LaConte, G. T. Yee and H. C. Dorn, Gd₃N@C₈₄(OH)_x: A new egg-shaped metallofullerene magnetic resonance imaging contrast agent, *J. Am. Chem. Soc.*, 2014, **136**, 2630–2636.
- 118 J. Zhang, P. P. Fatouros, C. Shu, J. Reid, L. S. Owens, T. Cai, H. W. Gibson, G. L. Long, F. D. Corwin, Z.-J. Chen and H. C. Dorn, High relaxivity trimetallic nitride (Gd₃N) metallofullerene MRI contrast agents with optimized functionality, *Bioconjugate Chem.*, 2010, **21**, 610–615.
- 119 T. Li, S. Murphy, B. Kiselev, K. S. Bakshi, J. Zhang, A. Eltahir, Y. Zhang, Y. Chen, J. Zhu, R. M. Davis, L. A. Madsen, J. R. Morris, D. R. Karolyi, S. M. LaConte, Z. Sheng and H. C. Dorn, A new interleukin-13 amino-coated gadolinium metallofullerene nanoparticle for targeted MRI detection of glioblastoma tumor cells, *J. Am. Chem. Soc.*, 2015, **137**, 7881–7888.
- 120 M. Rohrer, H. Bauer, J. Mintorovitch, M. Requardt and H.-J. Weinmann, Comparison of magnetic properties of MRI contrast media solutions at different magnetic field strengths, *Invest. Radiol.*, 2005, **40**, 715–724.
- 121 Z. Zhao, M. Zhen, C. Zhou, L. Li, W. Jia, S. Liu, X. Li, X. Liao and C. Wang, A gadofullerene based liver-specific MRI contrast agent for an early diagnosis of orthotopic hepatocellular carcinoma, *J. Mater. Chem. B*, 2021, **9**, 5722–5728.
- 122 Z. Han, X. Wu, S. Roelle, C. Chen, W. P. Schiemann and Z.-R. Lu, Targeted gadofullerene for sensitive magnetic resonance imaging and risk-stratification of breast cancer, *Nat. Commun.*, 2017, **8**, 692.
- 123 L. Xiao, T. Li, M. Ding, J. Yang, J. Rodríguez-Corrales, S. M. LaConte, N. Nacey, D. B. Weiss, L. Jin, H. C. Dorn and X. Li, Detecting chronic post-traumatic osteomyelitis of mouse tibia via an IL-13Rα2 targeted metallofullerene magnetic resonance imaging probe, *Bioconjugate Chem.*, 2017, **28**, 649–658.
- 124 D. M. Guldi, Capped fullerenes: stabilization of water-soluble fullerene monomers as studied by flash photolysis and pulse radiolysis, *J. Phys. Chem. A*, 1997, **101**, 3895–3900.
- 125 S. Laus, B. Sitharaman, É. Tóth, R. D. Bolskar, L. Helm, S. Asokan, M. S. Wong, L. J. Wilson and A. E. Merbach, Destroying gadofullerene aggregates by salt addition in aqueous solution of Gd@C₆₀(OH)_x and Gd@C₆₀[C(COOH₂)]₁₀, *J. Am. Chem. Soc.*, 2005, **127**, 9368–9369.
- 126 J. Murtagh, D. O. Frimannsson and D. F. O’Shea, Azide conjugatable and pH responsive near-infrared fluorescent imaging probes, *Org. Lett.*, 2009, **11**, 5386–5389.
- 127 M. Gao, F. Yu, H. Chen and L. Chen, Near-infrared fluorescent probe for imaging mitochondrial hydrogen polysulfides in living cells and in vivo, *Anal. Chem.*, 2015, **87**, 3631–3638.
- 128 S. Wang, Z. Zhou, Z. Wang, Y. Liu, O. Jacobson, Z. Shen, X. Fu, Z.-Y. Chen and X. Chen, Gadolinium metallofullerene-based activatable contrast agent for tumor signal amplification and monitoring of drug release, *Small*, 2019, **15**, 1900691.
- 129 Y. Li, R. Biswas, W. P. Kopcha, T. Dubroca, L. Abella, Y. Sun, R. A. Crichton, C. Rathnam, L. Yang, Y.-W. Yeh, K.

- Kundu, A. Rodríguez-Fortea, J. M. Poblet, K.-B. Lee, S. Hill and J. Zhang, Structurally defined water-soluble metallofullerene derivatives towards biomedical applications, *Angew. Chem., Int. Ed.*, 2022, DOI:10.1002/anie.202211704.
- 130 S. Wang, J. Lin, Z. Wang, Z. Zhou, R. Bai, N. Lu, Y. Liu, X. Fu, O. Jacobson, W. Fan, J. Qu, S. Chen, T. Wang, P. Huang and X. Chen, Core-satellite polydopamine-gadolinium-metallofullerene nanotheranostics for multimodal imaging guided combination cancer therapy, *Adv. Mater.*, 2017, **29**, 1701013.
- 131 S. Wang, Z. Zhou, G. Yu, N. Lu, Y. Liu, Y. Dai, X. Fu, J. Wang and X. Chen, Gadolinium metallofullerene-polypyrrole nanoparticles for activatable dual-modal imaging-guided photothermal therapy, *ACS Appl. Mater. Interfaces*, 2018, **10**, 28382–28389.
- 132 D. Chen, Y. Zhou, D. Yang, M. Guan, M. Zhen, W. Lu, M. E. Van Dort, B. D. Ross, C. Wang, C. Shu and H. Hong, Positron emission tomography/magnetic resonance imaging of glioblastoma using a functionalized gadofullerene nanoparticle, *ACS Appl. Mater. Interfaces*, 2019, **11**, 21343–21352.

f